Modulating the site-specific oral delivery of sorafenib using sugar-grafted nanoparticles for hepatocellular carcinoma treatment

Lakshmi Tunki, Hitesh Kulhari, Lakshma Nayak Vadithe, Madhusudana Kuncha, Suresh Bhargava, Deep Pooja, Ramakrishna Sistla

PII: S0928-0987(19)30241-6
DOI: https://doi.org/10.1016/j.ejps.2019.104978
Article Number: 104978
Reference: PHASCI 104978

To appear in: *European Journal of Pharmaceutical Sciences*

Received date: 6 April 2019
Revised date: 7 June 2019
Accepted date: 25 June 2019

Please cite this article as: L. Tunki, H. Kulhari, L.N. Vadithe, et al., Modulating the site-specific oral delivery of sorafenib using sugar-grafted nanoparticles for hepatocellular carcinoma treatment, European Journal of Pharmaceutical Sciences, https://doi.org/10.1016/j.ejps.2019.104978

Modulating the site-specific oral delivery of sorafenib using sugar-grafted nanoparticles for hepatocellular carcinoma treatment

Lakshmi Tunki[a,c], *Hitesh Kulhari*[b], *Lakshma Nayak Vadithe*[a], *Madhusudana Kuncha*[a], *Suresh Bhargava*[c], *Deep Pooja*[a,]*, *Ramakrishna Sistla*[a,]*

[a]Applied Biology Division, CSIR-Indian Institute of Chemical Technology, Hyderabad, Telangana 500007, India

[b]School of Nano Sciences, Central University of Gujarat, Gandhinagar, Gujarat 302030, India

[c]Centre for Advanced Materials and Industrial Chemistry, School of Science, RMIT University, Melbourne, VIC 3001, Australia

Corresponding Author

***Email:** sistla@iict.res.in, sistla@csiriict.in (R.S.), d.dpooja00@gmail.com (D.P.)

CSIR-IICT communication no: IICT/Pubs./2019/027.

ABSTRACT

Globally, one in six deaths is reported due to cancer suggesting the critical need for development of advanced treatment regimens. In this study, solid lipid nanoparticles (SLN) were prepared and appended with polyethylene glycol (PEGylated) galactose and a multikinase inhibitor sorafenib (SRFB) was used as chemotherapeutic drug, for treating hepatocellular carcinoma (HCC). The nanoparticles were evaluated for *in-vitro* and *in-vivo* performances to showcase the targeting efficiency and therapeutic benefits of the sorafenib loaded ligand conjugated nanoparticles

(GAL-SSLN). When compared with SRFB or Sorafenib loaded SLN, GAL-SSLN showed superior cytotoxicity and apoptosis in HepG2 (human hepatocellular carcinoma cells). In addition, *in-vivo* pharmacokinetics and real time biodistribution studies in BALB/c mice showed that the surface conjugation of nanoparticles with galactose resulted in better pharmacokinetic performance and targeted delivery of the nanoparticles to liver. Results indicated that GAL-SSLN showed promising attributes in terms of targeting sorafenib to liver and therapeutic efficacy.

KEYWORDS

PEGylated galactose, Solid lipid nanoparticles, Sorafenib, Hepatocellular carcinoma, Bioavailability, Targeting.

Graphical abstract

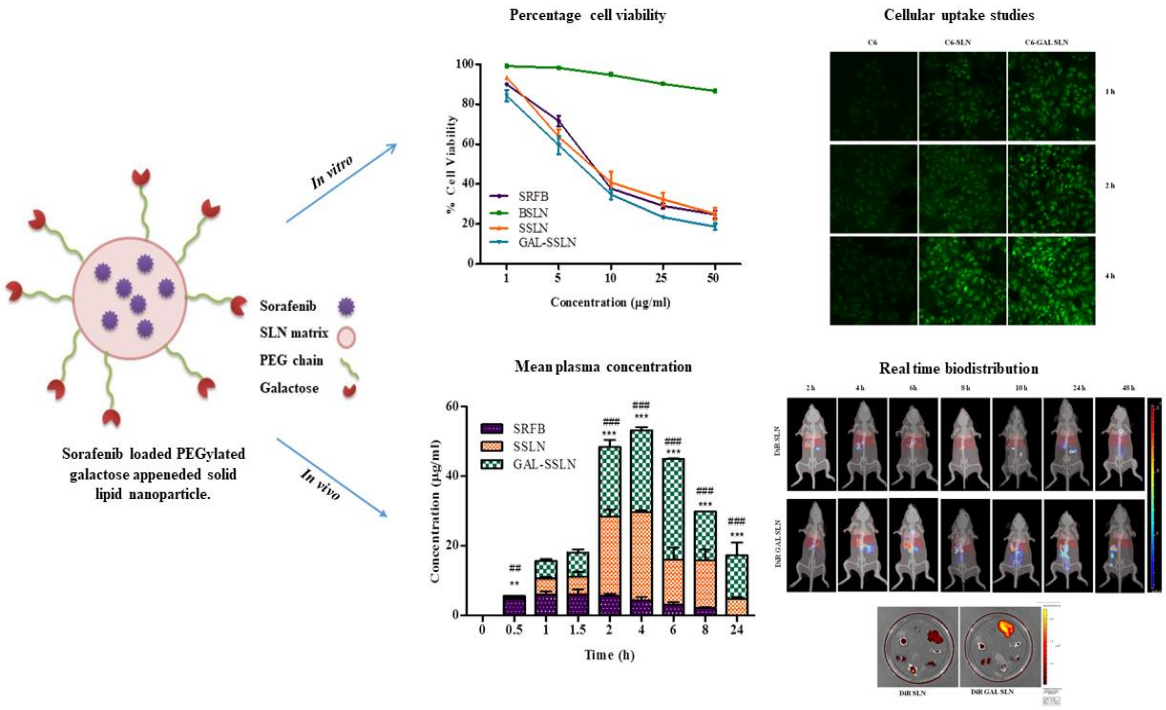

ABBREVIATIONS

^{1}HNMR, Proton nuclear magnetic resonance; DMEM, Dulbecco's modified eagle medium; DMSO, Dimethyl sulfoxide; DPBS, Dulbecco's phosphate buffered saline; DSC, Differential scanning calorimetry; EDC, 1-Ethyl-3-(3-dimethylaminopropyl) carbodiimide; EE, Encapsulation efficiency; FBS, Fetal bovine serum; FTIR, Fourier transform infrared spectroscopy; HPLC, High performance liquid chromatography; IC50, Half-maximal inhibitory concentration; MTT, 3-(4, 5- dimethylthiazol-2-yl)-2, 5-diphenyl tetrazolium bromide; NHS, N-hydroxysuccinimide; PBS, phosphate buffer saline; SAB, Sodium acetate buffer; SD, Standard deviation; VEGF, Vascular endothelial growth factor; SLN, Solid lipid nanoparticle; SRFB, Sorafenib; SSLN, SRFB loaded SLN; GAL-SSLN, SRFB loaded PEGylated galactose conjugated SLN; HepG2, human hepatocellular carcinoma cells; HCC, hepatocellular carcinoma; IARC, International Agency for Research on Cancer; PEG, Polyethylene glycol; CTLR, C-type lectin receptors; ASGPR, asialoglycoprotein receptor ligand; PDGF, platelet-derived growth receptors; GMS, Glyceryl monostearate; BSLN, Blank SLN; C6, coumarin-6; JC-1, 5,5,6,6-tetrachloro-1,1,3,3-tetraethylbenzimidazolocarbocyanine iodide; IAEC, Institutional Animal Ethics Committee; CPCSEA, Committee for the Purpose of Control and Supervision of Experiments on Animals; ACN, Acetonitrile; MeOH, Methanol; C_{max}, maximum plasma concentration; AUC, area under the curve; AUMC, area under the first moment curve plasma; t_{max}, time to reach peak plasma concentration; $t_{1/2}$, half-life; MRT, mean residence time; DiR, 1, 1′-Dioctadecyl-3,3,3′,3′-tetramethylindotricarbocyanine iodide; ANOVA, Analysis of variance.

1. Introduction

According to GLOBOCAN 2018 cancer statistics, International Agency for Research on Cancer (IARC) estimated about 18.1 million new cancer cases and 9.6 million cancer deaths across the world in 2018. Among these, liver or hepatocellular carcinoma would account for 8.2% of mortality rate (Bray et al., 2018). There is an increasing global burden of HCC and is expected to increase to 1 million cases per year in the coming years. Sorafenib (SRFB) is a FDA approved oral multikinase inhibitor and is used as first line chemotherapeutic treatment for patients with advanced HCC (Llovet et al., 2018). SRFB inhibits tumor cell proliferation by downregulating Ras oncogene activity and prevents angiogenesis via inhibiting vascular endothelial growth factor (VEGF) and platelet-derived growth (PDGF) receptors thus the progression of tumor is ceased (Wilhelm et al., 2006).

The major pitfall of conventional use of SRFB is its low aqueous solubility leading to low oral bioavailability (~8.43%) and thus low therapeutic efficacy (Zhang et al., 2014). Further, non-specific biodistribution of SRFB results in systemic adverse effects like gastrointestinal disturbances, low blood flow through heart, heart attack, hand-foot skin reaction, alterations in thyroid hormone levels, non-specific tissues uptake etc., affecting the quality life of patients and disrupting the treatment which further lead to compromised treatment. This suggests the need for development of an alternate delivery system that can take the edge off the above effects to large extent if not completely (Cervello et al., 2017; Cheng et al., 2009).

The present advanced technology in the field of medicine is nanomedicine, which is in boom in various fields of diagnosis, treatment and prevention. Nanomedicine claim to have

inimitable physicochemical properties that can be used to improve both pharmacokinetic and pharmacodynamic properties of the drug molecules (Wicki et al., 2015; Cai and Sheng, 2015). The art of encapsulating the drug in carrier and then anchoring it with targeting ligand is one of the current areas of research in cancer chemotherapy. This kind of approach is aimed at reducing the adverse side effects by directing the drug to reach the target organ. In addition, nanoparticles also release the encapsulated drug in controlled manner which helps in reducing the dose as well as number of doses.

In recent years, various formulations of sorafenib loaded nanoparticles were prepared and evaluated for anticancer efficacy both *in-vitro* and *in-vivo*. Yanhong Su et al., formulated biocompatible micelles for SRFB delivery and showed better antitumor activity with prolonged circulation time (Song et al., 2018). Xia sheng et al., prepared polymeric nanoparticles and showcased that SRFB encapsulated in nanoparticles showed higher therapeutic efficacy than the free SRFB (Sheng et al., 2017). In a study, anti-GPC3 antibody-tagged sorafenib loaded nanoparticles were developed to inhibit the growth of liver xenograft tumours (Tang et al., 2018). Melchiorre Cervello prepared nanoparticles loaded with sorafenib surface modified with brush copolymer which showed enhanced permeability into tumor and thus, improved therapeutic efficacy against Hep3B xenograft model in nude mice (Cervello et al., 2017).

In this present work, SRFB loaded solid lipid nanoparticles were formulated and to impart selectivity to the nanoparticles towards HCC. Galactose, a C-type lectin receptors (CTLR) binding ligand, was conjugated on the surface of nanoparticles. Asialoglycoprotein receptors (ASGPR) are one among the highly expressed CTLR in liver as well as in HCC cells and are known to least or minimally present on other cells (D'Souza and Devarajan, 2015). Among the various carbohydrate receptor ligands like N-acetylgalactosamine, lactose, mannose,

sialic acid, galactose etc, galactose is widely used as a targeting ligand against HCC because of its high targeting affinity (Richard J. Stockert, 1995; Hashida et al., 2001; Li et al., 2016; Oh et al., 2016; Kawakami and Hashida, 2014; Huang et al., 2018). Further, herein we synthesized and used poly(ethylene glycol) conjugated galactose as a liver directing ligand. PEGylation of nanoparticles with PEG having molecular weight of more than 2000 daltons offers the advantages like impediment of particle aggregation, and escaping their uptake by reticuloendothelial cells and thus, the increase in their circulation half-life (Ding et al., 2014; Otsuka et al., 2003). Therefore, a liver targeting, biocompatible drug delivery system was designed to improve the oral delivery and efficacy of SRFB in the form of SSLN and GAL-SSLN to treat HCC.

2. Materials and methods

2.1 Materials

Glyceryl monostearate (GMS) was obtained from Alfa Aesar (Johnson Matthey Chemicals, Hyderabad, India). Dialysis tubing (molecular weight cut off 12–14 and 2 kDa), thiazolyl blue tetrazolium bromide (MTT), stearic acid, N—(3—dimethylaminopropyl)—N'—ethylcarbodiimide (EDC), N—hydroxysuccinimide (NHS), poly(ethylene glycol) bis(amine) average molecular weight of 3400, dimethyl sulfoxide (DMSO), Hoechst 33258 and annexin V—FITC apoptosis detection kit were procured from Sigma–Aldrich (St., Louis, MO, USA). Lecithin soy was acquired from Himedia (Mumbai, India). Sorafenib tosylate (SRFB) was a gift from TherDose Pharma Pvt. Ltd., (Hyderabad, India). 1, 1′—Dioctadecyl—3,3,3′,3′—

tetramethylindotricarbocyanine iodide (DiR) was procured from Biotium (Hayward, CA). High performance liquid chromatography (HPLC) grade solvents such as chloroform, methanol and acetonitrile were purchased from Merck limited (Mumbai, India). HepG2 human liver cancer cells were obtained from American Type Culture Collection (ATCC) (Manassas, VA, USA). Dulbecco's modified eagle's media (DMEM), fetal bovine serum (FBS) and phosphate buffer saline (PBS) were bought from Gibco, USA. Tween 80 and D (+) galactose were products of sd Fine Chem Ltd. (Mumbai, India). Remaining chemicals and solvents were of analytical grade and used further without any purification.

2.2 Synthesis of PEGylated galactose conjugate

For opening galactose ring molecules and to generate aldehyde group, D-galactose (8 μM) was dissolved in 0.1 M sodium acetate buffer (pH 4) and kept at ambient temperature for 4 h (Kumar et al., 2006). After that, ring opened galactose was reacted with PEG-bis (amine) in 1:2 molar ratio in 0.1 M sodium tetraborate buffer, stirred magnetically for two days at ambient temperature. Finally, the formed PEGylated galactose was dialyzed using dialysis tubing of molecular weight cutoff 2 kDa against MilliQ water to remove unreacted compounds, lyophilized and stored at room temperature (Lim et al., 2000).

2.3 Characterization of PEGylated galactose conjugate

The formed conjugate was characterized using Fourier transform infrared analysis (FTIR) analysis using a FTIR spectrophotometer (Perkin Elmer, UK). Samples were mixed with KBr and compression pressed to form pellet. The pellet transmittance was measured by scanning wave number over a range of 400 to 4000 cm^{-1}. Proton NMR spectra of galactose, PEG-

bis(amine) and PEGylated galactose conjugate were observed using BRUKER DPX 300MHz spectrometer (Bruker, Karlsruhe, Germany). The samples were solubilized in D_2O.

2.4 Preparation of solid lipid nanoparticles

Emulsification and solvent evaporation method was used to prepare SLN as reported previously (Yuan et al., 2013). Briefly, 80 mg of GMS, 20 mg of stearic acid and 40 mg soy lecithin were dissolved in 2 mL of chloroform, acting as lipidic organic phase, transferred to 10 mL of aqueous surfactant phase composed of 1.5% w/v of Tween 80. This dispersion was homogenized (Ultra-turrax, Germany) at 11,000 rpm for 5 min. The formed coarse emulsion was further comminuted using the force of sonic waves by probe sonicator (vibra Cell, Sonics, USA) for 20 min. Finally, the obtained nanoemulsion was kept for stirring at 1000 rpm for 3 h on magnetic stirrer for formation of nanoparticles through solvent evaporation process. SLN were collected by centrifugation at 13,000 rpm for 45 min using centrifuge (Biofuge Stratos, Heraeus, Germany) (Pooja et al., 2016b). For the preparation of SRFB loaded SLN (SSLN), 4 mg of SRFB was dissolved in 0.2 mL of methanol and was incorporated into the organic lipidic phase.

2.5 Sorafenib encapsulation efficiency

Encapsulation efficiency of SRFB into SLN was determined by indirect method and employing a HPLC system (Waters, USA). Supernatant obtained after centrifugation of nanoparticle dispersion was used to determine the unencapsulated or free drug. The amount or percentage of encapsulated SRFB in nanoparticles was calculated by means of the formula, % encapsulation efficiency = [1-(Ds/Di)]×100, where Ds: amount of drug present in supernatant; Di: initial amount of drug added to formulate the SSLN. Determination of SRFB content was performed using reverse phase HPLC equipped with octadecylsilane (C18) column (Waters

Reliant, 5 µm, 4.6 ×250 mm) maintained at a temperature of 25±5 °C and photodiode array detector. A mobile phase containing mixture of acetonitrile and water (70:30, v/v), pumped at a flow rate of 1.0 mL/min, injection volume 20 µL and detection was set at a wavelength of 265 nm.

2.6. Surface conjugation of PEGylated Galactose to SSLN using carbodiimide reaction

PEGylated galactose was conjugated with its free amine group onto carboxylic acid group bearing SLN using carbodiimido coupling reaction (Pooja et al., 2016a). Briefly 50 mg of lyophilized formulation was dispersed in PBS pH 7.4 and 1 mL each of 0.1 M EDC/NHS were added and incubated for 2 h. SLN were then centrifuged at 13,000 rpm for 20 min to remove EDC and NHS. The collected nanoparticles were then dispersed in PBS, PEGylated galactose (50 mg) was added and conjugation was allowed by overnight incubation. The galactose conjugated nanoparticles were separated by centrifugation at 13,000 rpm for 30 min.

2.7 Characterization of nanoparticles

Particle size, polydispersity index (PDI) and zeta potential were determined for the blank solid lipid nanoparticles (BSLN), SSLN and GAL-SSLN using dynamic light scattering by particle size analyzer Nano-ZS (Malvern Instrument Ltd., UK). DSC analysis was performed to check the physical state of SRFB before and after encapsulation in SLN using DSC STAR ONE (Mettler, Switzerland). Thermograms of free SRFB and SSLN were obtained by scanning the samples (5 mg) sealed into aluminum pan from 30 °C to 300 °C at a speed of 10 °C/min, under nitrogen environment. FTIR of SRFB, lyophilized SSLN and GAL-SSLN was performed using FTIR spectrometer (Perkin Elmer, UK). Samples were prepared in KBr pellet and transmittance was measured ranging from 400 to 4000 cm^{-1}.

2.8 In-vitro drug release

In-vitro drug release studies were carried using dialysis bag method (molecular weight cutoff 12-14 kDa) and the release behavior of SRFB loaded formulations *viz.* SSLN and GAL-SSLN were compared with free SRFB. Different release media like sodium acetate buffer (SAB) pH 5.0, 0.1 N HCl pH 1.2, phosphate buffer pH 6.8 and saline (PBS) pH 7.4 were used for the studies. SRFB, SSLN or GAL-SSLN, equivalent to 1 mg, were suspended in 1 mL of 0.5 % Tween 80 solution, taken in dialysis bags and kept in 50 mL of drug release media containing 1% Tween 80 maintained at temperature of 37 ± 0.5 °C, were allowed to stir at 100 rpm. At specified time points (0.5, 1, 2, 4, 6, 8, 12, 24, 48 h), one mL of media was taken out and replaced with fresh media to maintain the sink conditions. These samples were then used for estimation of SRFB released into the media using HPLC instrument.

2.9 Anti proliferation assay

HepG2 human liver cancer cell were grown in DMEM (Dulbecco's Modified Eagle's medium), supplemented with 10% fetal bovine serum (FBS) in CO_2 incubator maintained at 37 °C and 5 % CO_2. Cells after trypsinization were harvested and seeded at 1×10^4 cells/well in 96 well plate and allowed for adhesion by incubating for 24 h. After which the cells were treated with SRFB formulations (SRFB, BSLN, SSLN, GAL-SSLN) at concentrations of 1, 5, 10, 25, 50 µg/mL and incubated for 48 h. Pure SRFB was dissolved in DMSO and further diluted with DMEM medium for making up of various dilutions. Thiazolyl blue tetrazolium bromide (MTT) at 5 mg/mL was added to each well at 10 µL volume and incubated further for 4 h, after which the media was removed and DMSO was added at volume of 100 µL to each well and absorbance was measured at 570 nm for the formed formazan crystals using multidetection microplate reader

(Synergy-4, Biotek, USA). Untreated cells grown under similar conditions were used as control for calculation of half-maximum inhibitory concentration (IC50) (Botta et al., 2007).

2.10 Nuclear fragmentation by Hoechst staining

HepG2 cells were seeded at a density of 10,000 cells over 18 mm cover slips and incubated for 24 h. Cells were treated with SRFB, SLN or GAL-SSLN at 5 and 10 µg/mL concentrations for 48 h. Hoechst 33258 was added to the cells at a concentration of 5 µg/mL and incubated for 30 min at 37 °C. Cells were washed with PBS and were observed under fluorescent microscope (Olympus microscope) to qualitatively determine the proportion of living and apoptotic cells based on their relative fluorescence and nuclear fragmentation (Kumar et al., 2017).

2.11 Annexin V-FITC assay

HepG2 (1×10^6) cells were seeded in six well plate and allowed to grow overnight. The medium was then replaced with complete medium containing SRFB, SSLN and GAL-SSLN at 5 and 10 µg/mL concentrations. After 48 h of treatment, cells were harvested by trypsinization, washed with PBS and centrifuged at 5000 rpm. Then the cells were stained with annexin V-FITC and propidium iodide using the annexin V-FITC apoptosis detection kit. Flow cytometry was used for analysis of apoptosis of the above treatments (Browne et al., 1991).

2.12 Cellular uptake study

Uptake of SLN formulations were studied by replacing the SRFB with a fluorescent probe i.e. coumarin-6 (C6). About 1×10^6 cells were seeded in 6-wells plate and allowed for adhering overnight in incubator. The cells were incubated with C6 alone, C6-SLN and C6-GAL

SLN at a concentration of 5 µg/mL. At specific time intervals of 1, 2 and 4 h the cells were observed for the uptake of nanoparticles using fully automated confocal laser-scanning microscopy (Olympus FluoView FV10i) (Kadari et al., 2017).

2.13 Determination of mitochondrial membrane potential (ΔΨm)

HepG2 (1×10^6 cells/well) cells were cultured in six well plates. After seeding, cells were treated with SRFB, SSLN and GAL-SSLN at 5 and 10 µg/mL concentrations. After 48 h of treatment, cells were collected by trypsinization and washed with PBS followed by resuspending in JC-1 (5,5,6,6-tetrachloro-1,1,3,3-tetraethylbenzimidazolocarbocyanine iodide) and incubated at 37 °C for 15 min. Cells were then subjected to flow cytometric analysis on a flow cytometer in the FL1, FL2 channel to detect mitochondrial membrane potential (Chakravarti et al., 2012).

2.14 Plasma pharmacokinetic study

In-vivo pharmacokinetic studies were performed in BALB/c mice; animal experimental procedure was permitted by the Institutional Animal Ethics Committee (IAEC) of the CSIR-Indian Institute of Chemical Technology, Hyderabad under the approval number (IICT/39/2017). Studies performed on mice were according to the guidelines of the Committee for the Purpose of Control and Supervision of Experiments on Animals (CPCSEA, Government of India). A week prior to performance of the studies animals were acclimatized in a biosafe house which is maintained at an ambient temperature of 22 ± 2 °C and relative humidity of 50−60% under a normal 12 h/12 h light/dark cycle.

One day before the experimentation animals were fasted overnight with water availability ad libitium. In total 36 animals were grouped randomly into three groups i.e. one for SRFB

suspension and others for SSLN and GAL-SSLN. The suspension of SRFB was prepared by dispersing the drug into 2% gum acacia whereas SLN formulations were prepared by dispersing them in normal saline. SRFB suspension or SLN formulations were administered to mice at a dose of 25 mg/Kg body weight through per oral gavage. Blood samples of approximate volume 0.3 mL were withdrawn at predetermined time points of (0.5, 1, 1.5, 2, 4, 6, 8 and 24 h) from retro-orbital plexus. Plasma was collected from blood samples after centrifugation at 2000 × g for 10 min. Collected plasma was immediately preserved at – 80 °C until further analysis using HPLC.

2.15 Plasma processing and analysis

For pharmacokinetic estimation of SRFB by HPLC, plasma samples were thawed to reach room temperature from which 90 µL of plasma aliquot was taken, to this 10 µL of erlotinib (1 mg/mL) was added as an internal standard and vortexed for 90 sec. Then, a volume of 400 µL of precipitating agent [ACN:MeOH (1:1 v/v)] was added, again vortexed for 120 sec, and then centrifuged at 10,000 rpm for 10 min at 22 °C temperature. The obtained supernatant was filtered through 0.2 µm filter and a volume of 20 µL was injected to the HPLC system for analysis at 265 nm. The pharmacokinetic parameters like maximum plasma concentration (C_{max}), area under the curve (AUC), area under the first moment curve plasma (AUMC), time to reach peak plasma concentration (t_{max}), half-life ($t_{1/2}$), clearance and mean residence time (MRT) were determined by employing drug concentration versus time curve using PK solver, a menu-driven add-in program for Microsoft Excel which is used for dealing with fundamental problems in pharmacokinetic and pharmacodynamic data analysis (Zhang et al., 2010).

2.16 Real time biodistribution studies using IVIS system

In-vivo imaging was carried out in BALB/c mice. To assess the fate of plain and targeted SLN after per oral administration, drug was replaced with real-time near infrared fluorophore (NIRF)-1,1′-Dioctadecyl-3,3,3′,3′-tetramethylindotricarbocyanine iodide (DiR) dye. Before the experiment, mice were fasted overnight and the next day DiR loaded formulations i.e., ligand free (DiR-SLN) and PEGylated galactose conjugated SLN (DiR-GAL SLN) were administered to mice through per oral route at 100 µL volume at dose of 0.5 mg/Kg of DiR. Distribution of the nanoparticles into various organs was monitored through fluorescence at regular, predetermined time points of 2, 4, 6, 8, 10, 24, and 48 h by anaesthetizing the mice using ketamine xylazine injection. After the last time point of the study i.e., 48 h, mice were sacrificed to reveal the fluorescence of various organs viz brain, heart, lungs, liver, kidneys, pancreas and spleen, using IVIS spectrum *in-vivo* imaging system (Caliper, MA, USA) (Song et al., 2018).

2.17 Statistical analysis

All the experiments were performed in triplicate (n=3), data was complied, analyzed using Graph Pad prism software (version 5), and data was expressed as mean ± standard deviation (SD). Comparison between groups were performed by using one way ANOVA applying Tukey's multiple comparison test and two way ANOVA through Bonferroni's post-test with (*$p < 0.05$, **$p < 0.01$ and ***$p < 0.001$). A value of $p > 0.05$ represents not significant.

3. Results

3.1 Synthesis and characterization of PEGylated galactose conjugate

The schematic representation of the conjugate synthesis is shown in **Figure 1**. Ring opened galactose having aldehyde functional group gets involved in bonding with one of the

amine groups in PEG bis (amine) and leads to formation of schiffs base (-N=CH-) which gets reduced to secondary amine (-NH-CH_2-) and both exist in equilibrium. PEGylated galactose formation was confirmed by the formation of schiffs base. The peak at 1415 cm^{-1} confirms the formation of schiffs base. The peaks at 1644 and 1562 cm^{-1} are due to stretching vibration of the imine (-C=N-H) group (**Figure 2(A)**) (Jain et al., 2015).

In ^{1}H-NMR, the signals for pure galactose were obtained at δ 4.7 ppm (D_2O), 4.15 ppm (–CH_2OH), 3.75, 3.61, 3.48 and 3.20 ppm (–CH_2 of ring), 2.79 – 1.90 ppm (–OH). The characteristic peaks for pure PEG bis (amine) could be observed at δ 7.30 ppm ($CDCl_3$), 1.45 to 2.2 ppm (–NH_2), 2.62 to 2.91 ppm (α-CH_2 of NH_2) and 3.61 to 4.53 ppm (β-CH_2). The chemical shift values shifted in PEGylated galactose conjugate can be clearly seen in ^{1}H-NMR spectra (**Figure 2(B)**). The conjugate showed chemical shift values at δ 4.7 ppm (D_2O), 4.12 to 3 ppm (–CH_2 of ring, β-CH_2 of PEG), 2.78 to 1.72 and 1.0 to 0.96 ppm (α-CH_2 of NH_2 and –OH of galactose ring). The appearance of chemical shift values at δ 3.14 to 3.02 ppm and 1.02 to 0.96 ppm confirmed the successful conjugation of galactose and PEG bis (amine).

3.2 Preparation of SRFB loaded solid lipid nanoparticles (SSLN and GAL-SSLN)

SLN were formulated by emulsification and solvent evaporation method where initial oil in water (O/W) emulsion is formed under homogenization. Inner organic phase was comprised of lipidic components like glyceryl monosterate for providing the solid matrix of SLN, stearic acid for bringing up the terminal functional carboxylic group (-COOH) and soy lecithin as an internal emulsifier. The formed coarse emulsion after homogenization was converted to nanoemulsion using sonic waves where they break up the larger oil globules into smaller size droplets after which the formed nanoemulsion was solvent evaporated for hardening and size reduction of the

SLN. Similarly, for making of SSLN, SRFB was dissolved in methanol and added to organic phase. For surface grafting of PEGylated galactose on the formed SSLN, EDC/NHS coupling reaction was used to form an amide between carboxylic group of SLN and amine group of PEGylated galactose.

3.3 Physicochemical characterization of nanoparticles

The average particle size of BSLN, SSLN and GAL-SSLN were 59.31±2.99, 68.36±3.14 and 111.00±6.99 nm respectively (**Table 1**). The surface conjugation of galactose on SLN brought an increase of nearly 50 nm in size. All formulations showed narrow polydispersity index and good zeta potential in the range of 0.209±0.022, 0.228±0.012, 0.354±0.024 and -20.9±1.41, -20.13±1.35, -19.8±1.11 mV respectively for BSLN, SSLN and GAL-SSLN formulations. Analytical HPLC chromatography for sorafenib showed the peak at retention time of 6.7 min. The encapsulation efficiency of SSLN and GAL-SSLN was found to be similar (97±1.5 and 95±1.8 respectively) indicating the no or minimal loss of drug during galactose surface conjugation to SSLN.

FTIR analysis of the SRFB showed characteristic peaks at 1724, 1458, 1183 and 937 cm^{-1} which were also observed in SSLN and GAL-SSLN indicating the encapsulation of SRFB into both the formulations. In addition, the carboxylic acid group peak observed at 1730 cm^{-1} in SSLN while amide peaks at 1647 and 1561 cm^{-1} are observed in GAL-SSLN, confirming the formation of amide bond between the nanoparticles and the ligand. DSC analysis of pure SRFB showed peak at 243 °C corresponding to its melting point. The absence of this endothermic peak in SSLN indicated the encapsulation of drug in amorphous form and homogenous dispersity of the drug in the lipid matrix (**Figure 3(A-C)**).

3.4 In-vitro drug release profile

In-vitro drug release studies were performed for pure SRFB, SSLN and GAL-SSLN in different media like 0.1 N HCl (pH 1.2), phosphate buffer pH 6.8, SAB pH (5.0) and PBS pH 7.4, representing the pH conditions of stomach, small intestine, tumor microenvironment and circulation fluid respectively to reveal the release blueprint of drug from SLN after oral administration. Pure drug solution showed almost complete release (> 95%) in all media within 8 h whereas the SRFB release from SLN showed only 25-40% release for the same 8 h time in different media suggesting the sustained release pattern of SRFB from the lipid matrix (**Figure 4**).

3.5 Induction of anti proliferation

Cell viability studies were performed against HepG2 cells for various formulations *viz* SRFB, BSLN, SSLN and GAL-SSLN to explore the cytotoxicity behavior of the SRFB in free as well as encapsulated form. The half inhibitory concentrations (IC50) of all the formulations are shown in **Table 2** and cell viability versus concentration graph shown in **Figure 5**. Both SSLN and GAL-SSLN showed IC50 values of 9.77±1.47 and 6.57±0.58 respectively in comparison with SRFB showing 9.48±0.45 ug/mL.

3.6 SRFB loaded nanoparticles induced apoptosis in human liver cancer cells

Apoptosis is one of the major pathways that lead to the cell death. Chromatin condensation and fragmented nuclei are known as the classic characteristics of apoptosis. It was considered of interest to investigate the apoptosis inducing effect of SRFB, SSLN and GAL-SSLN by Hoechst 33258 staining in HepG2 cells. Cells were treated with formulations at 5 and 10 µg/mL concentrations for 48 h. Results indicated that nanoparticle formulations showed

potent effect on nuclear condensation and fragmentation when compared with untreated control cells and the results also demonstrated that GAL-SSLN was better than SSLN in exerting the cellular apoptosis (**Figure 6**).

The apoptotic effect of SRFB, SSLN and GAL-SSLN was further evaluated by annexin V–FITC/propidium iodide dual staining assay to examine the externalization of phosphatidylserine and to comprehend whether it is due to physiological apoptosis or nonspecific necrosis (Konstantinov and Berger, 1999). In this study, HepG2 cells were treated with SRFB, SSLN and GAL-SSLN for 48 h at 5 and 10 µg/mL concentrations to examine the apoptotic effect. It was observed that these formulations showed significant apoptosis against HepG2 cells as shown in **Figure 7**. Results indicated that SRFB, SSLN and GAL-SSLN showed 26.19, 24.48 and 33.03 % of apoptosis at 5 µg concentration whereas they showed 58.21, 48.56 and 63.29 % of apoptosis at 10 µg concentration respectively. These results clearly demonstrated that GAL-SSLN was effective in inducing higher cellular apoptosis compared to SSLN or SRFB alone.

3.7 Cellular uptake study

Fluorescent nanoparticles (C6-SLN and C6-GAL SLN) were prepared by loading C6 in place of sorafenib to determine the uptake of SLN by HepG2 cells. After the incubation times of 1, 2, and 4 h with C6 alone, C6-SLN and C6-GAL SLN the green signal of C6 in the cells was observed and it was found that at all the time points C6-GAL SLN showed higher uptake than C6-SLN. Further, the uptake of nanoparticles was also time dependent as the intensity of green fluorescence was increased at each subsequent time point. These results clearly indicated that the presence of ASGPR on HepG2 cells aids in augmented uptake of C6-GAL SLN in comparison to C6-SLN (**Figure 8**).

3.8 Effect of SRFB loaded nanoparticles on the mitochondrial membrane potential (ΔΨm)

The maintenance of mitochondrial membrane potential (ΔΨm) is important for mitochondrial integrity and bioenergetic function (Gonda et al., 2008). Mitochondrial changes, including loss of ΔΨm are key proceedings that take place during drug induced apoptosis. To learn the apoptosis inducing effect of SRFB, SSLN and GAL SSLN mitochondrial membrane potential (ΔΨm) changes were detected using the fluorescent probe JC-1 (5,5,6,6-tetrachloro 1,1,3,3-tetraethylbenzimidazolocarbocyanine iodide-5 mg/mL). The red fluorescence and green fluorescence were detected at FL-2 and FL-1 channel, respectively. During apoptosis ΔΨm decreases and is measured by decrease in the ratio of red fluorescence (FL-2) to green fluorescence (FL-1). After 48 h of treatment, it was observed that the ΔΨm of HepG2 cells is reduced in case of all formulations but the reduction was the highest with GAL-SSLN (**Figure 9**).

3.9 Plasma Pharmacokinetic study

To study the *in-vivo* pharmacokinetic response of various prepared formulations i.e. SRFB suspension, SSLN and GAL-SSLN were administered to BALB/c mice. **Figure 10** shows the graph plotted between mean plasma concentration and time profiles for three formulations. The data of different pharmacokinetic parameters were analyzed by non-compartmental analysis using PK solver and are presented in **Table 3**. The maximum plasma concentration C_{max} of pure SRFB, SSLN and GAL-SSLN was 6.75±1.07, 25.22±0.50 and 28.90±0.13 μg/mL, respectively. In case of SRFB suspension, drug was not detectable in plasma after 8 h whereas of the drug released from both SSLN and GAL-SSLN was detectable up to 24 h. The reason can be explained that pure SRFB is having low solubility and thus gets eliminated from the body

whereas the drug loaded into SLN showed enhanced plasma concentration because the drug gets protected into solid lipid matrix and gets absorbed well through payer's patches present in M cells (Pooja et al., 2016a). This enhanced absorption in turn leads to improved AUC (an indicator of extent of absorption) where SSLN (272.05±30.60 µg/mL*h) and GAL-SSLN (363.09±32.74 µg/mL*h) showed significantly higher values ($p<0.001$) when compared with free SRFB. Clearance of SRFB was significantly reduced in case of both SSLN (7.8 fold) and GAL-SSLN (18.3 fold) because of increased circulation time. In particular, GAL-SSLN showed drastic decrease in clearance that can be accounted to the presence of PEG as a spacer molecule between galactose and SLN. PEGylation offers numerous advantages and is well known to extend the circulation time of nanoparticles (Yuan et al., 2013). Results obtained from the pharmacokinetic analysis confirm the improved drug delivery efficiency of the GAL-SSLN when compared to free SRFB.

3.10 Real time biodistribution of nanoparticles

The targeting ability of the synthesized conjugate towards liver was explored by *in-vivo* biodistribution studies in BALB/c mice using a non-invasive imaging system. Near infrared active dye (DiR)-loaded nanoparticles (DiR-SLN and DiR-GAL SLN) were prepared and administered orally to the animals. In general, SLN have natural tendency to go and lodge in lungs with the increase in time after oral administration (Pooja et al., 2016a). A similar kind of distribution was observed in this study where unconjugated DiR-SLN were observed in the lungs of the treated animals. In contrary, GAL-mediated, targeted nanoparticles were observed in liver even after 48 h of incubation. *Ex-vivo* fluorescence performed at the end of 48 h showed strong fluorescence intensity in liver in case of DiR-GAL SLN whereas the plain DiR-SLN showed affinity towards lungs. This clearly indicates that the SLN conjugated with galactose showed

targeting towards liver whereas the unconjugated SLN showed towards lungs (Pooja et al 2016a; Du et al., 2010; van Rijt et al., 2014) (**Figure 11(A, B)**).

4. Discussion

The drawbacks of SRFB were subdued in the present study wherein SRFB loaded and PEGylated galactose conjugated SLN were formulated with high drug encapsulation efficiency. Nanoparticles in the size range of 10-150 nm were known to be as successful delivery vehicles that will also ensure extended circulation time and tumor accumulation. Both SSLN and GAL-SSLN were formulated below 150 nm that will support in increasing circulation time and tumor assembling (Steichen et al., 2013). Drug release patterns of both SSLN and GAL-SSLN showed similar biphasic release indicating the initial burst release followed by persistent release which was in well agreement with our previous findings using hydrophobic drugs loaded into SLN (Pooja et al., 2016a; Pooja et al., 2015a; Pooja et al., 2015b). The cytotoxicity effect of formulations, clearly indicated that BSLN was non-toxic and cells incubated with BSLN showed good proliferation at all concentrations indicating that the employed lipid carriers are biocompatible and nontoxic. Moreover, the anticancer efficacy of SRFB was improved upon encapsulation in GAL-SSLN indicating that conjugation of galactose in PEGylated form on SLN improved its cytotoxic effect by means of increasing the penetrability of SRFB through receptor mediated endocytosis (Ding et al., 2014; Ma et al., 2018; Huang et al., 2018).

The intracellular uptake studies of the C6-GAL SLN showed enhanced intracellular localization in comparison to C6-SLN and C6. This study reveals the fact that PEG molecules act like a spacer between the galactose and SLN also helps in binding with head groups of phospholipids chain of cell membranes which aid in more penetration (Yamazaki and Ito, 1990).

In essence, the cellular uptake study was well in accordance with the cytotoxicity results which indicate that ligand conjugated SLN showed higher uptake and hence, increased cytotoxicity in respect to unconjugated SLN (Ding et al., 2014; Ma et al., 2018; Huang et al., 2018).

For pharmacokinetic studies, pure SRFB was compared with both SSLN and GAL-SSLN. The prolonged retention of SRFB encapsulated inside both SSLN and GAL-SSLN in blood circulation also enhances its chance of reaching to targeting cells thereby extracting the maximum benefit at the given concentration. Moreover, this enhanced bioavailability of the drug through GAL-SSLN also helps in reducing the dose in given dosage regimen. Real time biodistribution studies clearly confirmed that the formulation i.e. DiR-GAL SLN was successfully targeted to liver since galactose residues were recognized by specific ASGPR present on liver. In addition, the PEGylation of the galactose showed increase in the circulation half-life and stability of the SLN.

5. Conclusion

SRFB encapsulation into SLN and use of PEGylated galactose as aiming ligand aid in improving various parameters like cytotoxicity, intracellular uptake and apoptotic activities on HepG2 cells. Although *in-vivo* studies were performed in normal BALB/c mice, results showcased the ability of the GAL-SSLN to deliver SRFB to liver and thus minimizing the non-specificity. Further, at the same time the newly developed ligand conjugated SLN displayed increased circulation half-life and thus, enhancing the chances of reducing the dose as well as number of administrations thereby an improvement in the patience compliance. Overall, the oral bioavailability of the SRFB can be improved by encapsulating it in SLN and grafting it with

PEGylated galactose. These results may open up an area for development of PEGylated galactose grafted nanoparticles for targeting hepatocellular carcinoma.

FIGURES

Figure 1: Schematic representation for synthesis of PEGylated galactose from ring opened galactose and PEG bis amine.

Figure 2: Characterization of PEGylated Galactose conjugate by A) FTIR B) NMR.

Figure 3: Physicochemical characterization of different sorafenib formulations. A) Particle size and Zeta potential of blank SLN (BSLN), sorafenib loaded SLN (SSLN) and galactose conjugated sorafenib loaded SLN (GAL-SSLN) measured by DLS. B) FTIR of sorafenib and GAL-SSLN. c) DSC thermograph of sorafenib and SSLN.

Figure 4: *In-vitro* drug release studies of sorafenib (SRFB), sorafenib loaded SLN (SSLN) and galactose conjugated sorafenib loaded SLN (GAL-SSLN) in A) sodium acetate buffer (SAB) pH 5.0 B) phosphate buffer saline (PBS) pH 7.4, C) 0.1N HCl pH 1.2 and D) phosphate buffer pH 6.8

Figure 5: Cell viability versus concentration curve on HepG2 cells incubated with different formulations viz., blank SLN (BSLN), sorafenib (SRFB), sorafenib loaded SLN (SSLN) and Galactose conjugated sorafenib loaded SLN (GAL-SSLN) after 48 h of incubation.

Figure 6: Hoechst staining on HepG2 cells for sorafenib (SRFB), sorafenib loaded SLN (SSLN) and Galactose conjugated sorafenib loaded SLN (GAL-SSLN) after 48 h of incubation. (A: Control, B and C: SRFB at 5 and 10 ug, D and E: SSLN at 5 and 10 ug, F and G: GAL-SSLN at 5 and 10 ug)

Figure 7: Annexin V-FITC apoptosis assay on HepG2 cells for sorafenib (SRFB), sorafenib loaded SLN (SSLN) and Galactose conjugated sorafenib loaded SLN (GAL-SSLN) after 48 h of

incubation. (A: Control, B and C: SRFB at 5 and 10 ug, D and E: SSLN at 5 and 10 ug, F and G: GAL-SSLN at 5 and 10 ug)

Figure 8: Cellular uptake studies for native coumarin-6 (C6) (5 µg/ml), coumarin-6 loaded SLN (C6-SLN) and coumarin-6 loaded galactose conjugated SLN (C6-GAL SLN) (5µg/ml) in HepG2 cells at different time intervals of 1, 2 and 4 h by confocal microscopy at 40X magnification.

Figure 9: Mitochondrial membrane potential (ΔΨm) on HepG2 cells for sorafenib (SRFB), sorafenib loaded SLN (SSLN) and Galactose conjugated sorafenib loaded SLN (GAL-SSLN). Formulations triggers mitochondrial injury. Drop in membrane potential (ΔΨm) was assessed by JC-1 staining. Samples were then subjected to flowcytometry analysis on a FACScan (Becton Dickinson) in the FL1, FL2 channel to detect mitochondrial potential. (A: Control, B and C: SRFB at 5 and 10 ug, D and E: SSLN at 5 and 10 ug, F and G: GAL- SSLN at 5 and 10 ug)

Figure 10: Mean plasma drug concentration of sorafenib (SRFB), Sorafenib loaded SLN (SSLN), galactose conjugated sorafenib loaded SLN (GAL-SSLN) at various time points of 0.5, 1, 2, 4, 6, 8, 24 h after per oral administration. Data represented as mean ± SD (n = 3, * represents comparison of SRFB with SSLN, # represents comparison of SRFB with GAL-SSLN and */ # $p < 0.05$, **/ ## $p < 0.01$ and ***/### $p < 0.001$)

Figure 11: The *in-vivo* fluorescence real time imaging and biodistribution studies of DiR loaded solid lipid nanoparticles (DiR-SLN) and galactose conjugated DiR loaded solid lipid nanoparticles (DiR-GAL SLN) after oral administration in BALB/c mice. (DiR: 1,11-Dioctadecyl-3,3,31,31-tetramethylindotricarbocyanine iodide) A) *In-vivo* fluorescence images of the mice at different time points. B) *ex-vivo* fluorescence images of vital organs (heart, liver, spleen, pancreas, lung, brain and kidney) at 48 h post injection.

TABLES

Table 1. Physicochemical characterization of empty solid lipid nanoparticles (BSLN), sorafenib loaded nanoparticles (SSLN) and galactose conjugated SSLN (mean ± standard deviation; n = 3).

Formulation	Particle size (d.nm)	Polydispersity index	Zeta potential (mV)	Drug encapsulation efficiency (%)
BSLN	**59.31±2.99**	**0.209±0.022**	**-20.9±1.41**	**-**
SSLN	**68.36±3.14**	**0.228±0.012**	**-20.13±1.35**	**97±1.5**
GAL-SSLN	**111±6.99**	**0.354±0.024**	**-19.8±1.11**	**95±1.8**

Table 2. Half maxillary inhibitory concentration (IC50) values of sorafenib (SRFB), SRFB loaded nanoparticles (SSLN) and galactose conjugated SSLN (GAL-SSLN) against HepG2 human hepatocellular carcinoma cell line after 48 h of incubation.

Formulation	IC50 at 48h (µg/ml)
SRFB	**9.48±0.45**
BSLN	**> 100 (193.70±1.46)**
SSLN	**9.77±1.47[a]**
GAL-SSLN	**6.57±0.58[*]**

* represents comparison between SRFB *vs* SSLN and GAL-SSLN. [a] represents insignificant difference in comparison with SRFB and *p < 0.05, **p < 0.01 and ***p < 0.001.

Table 3. Pharmacokinetic parameters of sorafenib (SRFB), sorafenib loaded SLN (SSLN), galactose conjugated sorafenib loaded SLN (GAL-SSLN).

PK Parameter	Unit	SRFB	SSLN	GAL-SSLN
C max	µg/ml	6.75±1.07	25.22±0.50***	28.90±0.13$^{***, \#\#}$
t max	h	1.17±0.28	4.00±0.00***	6.00±0.00$^{***, \#\#\#}$
AUC $_{0-t}$	µg/ml*h	32.59±2.98	272.05±30.60***	363.09±32.74$^{***, \#}$
AUC $_{0-\alpha}$	µg/ml*h	45.88±3.87	357.20±25.35***	598.92±36.28$^{***, \#\#\#}$
AUMC $_{0-\alpha}$	µg/ml*h^2	326.10±23.78	6723.35±52.36**	14896.37±496.08$^{***, \#\#}$
MRT	h	6.58±0.58	16.65±3.64**	26.49±1.58$^{***, \#}$
Clearance	(µg/ml)/h	0.55±0.04	0.07±0.004***	0.03±0.01$^{***, a}$
$t_{1/2}$	h	4.36±0.20	14.07±0.06***	16.75±1.09$^{***, \#}$

C_{max} = peak plasma concentration, t_{max} = time to reach peak plasma concentration, AUC = area under the curve, AUMC = area under the first moment curve, MRT = mean residence time, $t_{1/2}$ = plasma half life. Data represented as mean ± SD, n = 3 (* represents comparison of SRFB with SSLN, # represents comparison of SRFB with GAL-SSLN, ^{a} indicates insignificant difference and */ # $p < 0.05$, **/ ## $p < 0.01$ and ***/### $p < 0.001$).

ACKNOWLEDGMENT

Authors thank Director, CSIR-Indian Institute of Chemical Technology, Hyderabad for providing the necessary facilities and support. Authors are grateful to M/s Therdose Pharma for providing sorafenib as gift sample. Lakshmi Tunki is thankful to the Director of the IICT-RMIT Research Centre for providing PhD scholarships.

Author Contributions

The manuscript was written through contributions of all authors. All authors have given approval to the final version of the manuscript.

Notes

Authors declare no conflict of interest for this manuscript.

REFERENCES

Botta, M., Armaroli, S., Castagnolo, D., Fontana, G., Pera, P., Bombardelli, E., 2007. Synthesis and biological evaluation of new taxoids derived from 2-deacetoxytaxinine J. Bioorg. Med. Chem. Lett. 17, 1579–1583. https://doi.org/https://doi.org/10.1016/j.bmcl.2006.12.101

Bray, F., Ferlay, J., Soerjomataram, I., 2018. Global Cancer Statistics 2018 : GLOBOCAN Estimates of Incidence and Mortality Worldwide for 36 Cancers in 185 Countries 394–424. https://doi.org/10.3322/caac.21492

Browne, L.J., Gude, C., Rodriguez, H., Steele, R.E., Bhatnager, A., 1991. Fadrozole hydrochloride: a potent, selective, nonsteroidal inhibitor of aromatase for the treatment of estrogen-dependent disease. J. Med. Chem. 34, 725–736. https://doi.org/10.1021/jm00106a038

Cai, L.-T., Sheng, Z.-H., 2015. Advances in cancer nanomedicine. Cancer Biol. Med. 12, 141–142. https://doi.org/10.7497/j.issn.2095-3941.2015.0049

Cervello, M., Pitarresi, G., Volpe, A.B., Porsio, B., Balasus, D., Emma, M.R., Azzolina, A., Puleio, R., Loria, G.R., Puleo, S., Giammona, G., 2017. Nanoparticles of a polyaspartamide-based brush copolymer for modified release of sorafenib: In vitro and in vivo evaluation. J. Control. Release 266, 47–56.

https://doi.org/10.1016/j.jconrel.2017.09.014

Chakravarti, B., Maurya, R., Siddiqui, J.A., Kumar Bid, H., Rajendran, S.M., Yadav, P.P., Konwar, R., 2012. In vitro anti-breast cancer activity of ethanolic extract of Wrightia tomentosa: Role of pro-apoptotic effects of oleanolic acid and urosolic acid. J. Ethnopharmacol. 142, 72–79. https://doi.org/https://doi.org/10.1016/j.jep.2012.04.015

Cheng, A.-L., Kang, Y.-K., Chen, Z., Tsao, C.-J., Qin, S., Kim, J.S., Luo, R., Feng, J., Ye, S., Yang, T.-S., Xu, J., Sun, Y., Liang, H., Liu, J., Wang, J., Tak, W.Y., Pan, H., Burock, K., Zou, J., Voliotis, D., Guan, Z., 2009. Efficacy and safety of sorafenib in patients in the Asia-Pacific region with advanced hepatocellular carcinoma: a phase III randomised, double-blind, placebo-controlled trial. Lancet Oncol. 10, 25–34. https://doi.org/10.1016/S1470-2045(08)70285-7

D'Souza, A.A., Devarajan, P. V, 2015. Asialoglycoprotein receptor mediated hepatocyte targeting — Strategies and applications. J. Control. Release 203, 126–139. https://doi.org/https://doi.org/10.1016/j.jconrel.2015.02.022

Ding, Y., Liang, J.J., Geng, D.D., Wu, D., Dong, L., Shen, W. Bin, Xia, X.H., Zhang, C., 2014. Development of a liver-targeting gold-PEG-galactose nanoparticle platform and a structure-function study. Part. Part. Syst. Charact. 31, 347–356. https://doi.org/10.1002/ppsc.201300120

Du, B., Yan, Y., Li, Y., Wang, S., Zhang, Z., 2010. Preparation and passive target of 5-fluorouracil solid lipid nanoparticles. Pharm. Dev. Technol. 15, 346–353. https://doi.org/10.3109/10837450903246390

Gonda, K., Tsuchiya, H., Sakabe, T., Akechi, Y., Ikeda, R., Nishio, R., Terabayashi, K., Ishii, K., Matsumi, Y., Ashla, A.A., Okamoto, H., Takubo, K., Matsuoka, S., Watanabe, Y., Hoshikawa, Y., Kurimasa, A., Shiota, G., 2008. Synthetic retinoid CD437 induces mitochondria-mediated apoptosis in hepatocellular carcinoma cells. Biochem. Biophys. Res. Commun. 370, 629–633. https://doi.org/https://doi.org/10.1016/j.bbrc.2008.04.008

Hashida, M., Nishikawa, M., Yamashita, F., Takakura, Y., 2001. Cell-specific delivery of genes with glycosylated carriers. Adv. Drug Deliv. Rev. 52, 187–196. https://doi.org/https://doi.org/10.1016/S0169-409X(01)00209-5

Huang, K.-W., Lai, Y.-T., Chern, G.-J., Huang, S.-F., Tsai, C.-L., Sung, Y.-C., Chiang, C.-C., Hwang, P.-B., Ho, T.-L., Huang, R.-L., Shiue, T.-Y., Chen, Y., Wang, S.-K., 2018. Galactose Derivative-Modified Nanoparticles for Efficient siRNA Delivery to Hepatocellular Carcinoma. Biomacromolecules 19, 2330–2339. https://doi.org/10.1021/acs.biomac.8b00358

Jain, A., Kesharwani, P., Garg, N.K., Jain, A., Jain, S.A., Jain, A.K., Nirbhavane, P., Ghanghoria, R., Tyagi, R.K., Katare, O.P., 2015. Galactose engineered solid lipid nanoparticles for targeted delivery of doxorubicin. Colloids Surfaces B Biointerfaces 134, 47–58. https://doi.org/https://doi.org/10.1016/j.colsurfb.2015.06.027

Kadari, A., Gudem, S., Kulhari, H., Bhandi, M.M., Borkar, R.M., Kolapalli, V.R.M., Sistla, R., 2017. Enhanced oral bioavailability and anticancer efficacy of fisetin by encapsulating as inclusion complex with HPβCD in polymeric nanoparticles. Drug Deliv. 24, 224–232. https://doi.org/10.1080/10717544.2016.1245366

Kawakami, S., Hashida, M., 2014. Glycosylation-mediated targeting of carriers. J. Control.

Release 190, 542–555. https://doi.org/https://doi.org/10.1016/j.jconrel.2014.06.001

Konstantinov, S.M., Berger, M.R., 1999. Human urinary bladder carcinoma cell lines respond to treatment with alkylphosphocholines. Cancer Lett. 144, 153–160. https://doi.org/https://doi.org/10.1016/S0304-3835(99)00219-0

Kumar, N.P., Sharma, P., Reddy, T.S., Nekkanti, S., Shankaraiah, N., Lalita, G., Sujanakumari, S., Bhargava, S.K., Naidu, V.G.M., Kamal, A., 2017. Synthesis of 2,3,6,7-tetramethoxyphenanthren-9-amine: An efficient precursor to access new 4-aza-2,3-dihydropyridophenanthrenes as apoptosis inducing agents. Eur. J. Med. Chem. 127, 305–317. https://doi.org/https://doi.org/10.1016/j.ejmech.2017.01.001

Kumar, P.V., Asthana, A., Dutta, T., Jain, N.K., 2006. Intracellular macrophage uptake of rifampicin loaded mannosylated dendrimers. J. Drug Target. 14, 546–556. https://doi.org/10.1080/10611860600825159

Li, M., Zhang, W., Wang, B., Gao, Y., Song, Z., Zheng, Q.C., 2016. Ligand-based targeted therapy: a novel strategy for hepatocellular carcinoma. Int. J. Nanomedicine 11, 5645–5669. https://doi.org/10.2147/IJN.S115727

Lim, D.W., Yeom, Y. Il, Park, T.G., 2000. Poly(DMAEMA-NVP)-b-PEG-galactose as Gene Delivery Vector for Hepatocytes. Bioconjug. Chem. 11, 688–695. https://doi.org/10.1021/bc000014u

Llovet, J.M., Montal, R., Sia, D., Finn, R.S., 2018. Molecular therapies and precision medicine for hepatocellular carcinoma. Nat. Rev. Clin. Oncol. https://doi.org/10.1038/s41571-018-0073-4

Ma, B., Lu, M., Yu, B.-Y., Tian, J., 2018. A galactose-mediated targeting nanoprobe for intracellular hydroxyl radical imaging to predict drug-induced liver injury. RSC Adv. 8, 22062–22068. https://doi.org/10.1039/C8RA01424H

Oh, H.R., Jo, H.-Y., Park, J.S., Kim, D.-E., Cho, J.-Y., Kim, P.-H., Kim, K.-S., 2016. Galactosylated Liposomes for Targeted Co-Delivery of Doxorubicin/Vimentin siRNA to Hepatocellular Carcinoma. Nanomater. (Basel, Switzerland) 6, 141. https://doi.org/10.3390/nano6080141

Otsuka, H., Nagasaki, Y., Kataoka, K., 2003. PEGylated nanoparticles for biological and pharmaceutical applications. Adv. Drug Deliv. Rev. 55, 403–419. https://doi.org/https://doi.org/10.1016/S0169-409X(02)00226-0

Pooja, D., Kulhari, H., Kuncha, M., Rachamalla, S.S., Adams, D.J., Bansal, V., Sistla, R., 2016a. Improving Efficacy, Oral Bioavailability, and Delivery of Paclitaxel Using Protein-Grafted Solid Lipid Nanoparticles. Mol. Pharm. 13, 3903–3912. https://doi.org/10.1021/acs.molpharmaceut.6b00691

Pooja, D., Kulhari, H., Tunki, L., Chinde, S., Kuncha, M., Grover, P., Rachamalla, S.S., Sistla, R., 2015a. Nanomedicines for targeted delivery of etoposide to non-small cell lung cancer using transferrin functionalized nanoparticles. RSC Adv. 5, 49122–49131. https://doi.org/10.1039/C5RA03316K

Pooja, D., Tunki, L., Kulhari, H., Reddy, B.B., Sistla, R., 2016b. Optimization of solid lipid nanoparticles prepared by a single emulsification-solvent evaporation method. Data Br. 6, 15–19. https://doi.org/https://doi.org/10.1016/j.dib.2015.11.038

Pooja, D., Tunki, L., Kulhari, H., Reddy, B.B., Sistla, R., 2015b. Characterization, biorecognitive activity and stability of WGA grafted lipid nanostructures for the controlled delivery of Rifampicin. Chem. Phys. Lipids 193, 11–17. https://doi.org/https://doi.org/10.1016/j.chemphyslip.2015.09.008

Richard J. Stockert, 1995. The Asialoglycoprotein Receptor : Relationships Structure , Function , and Expression Between. Physiol. Rev. 75, 591–609.

Sheng, X., Huang, T., Qin, J., Li, Q., Wang, W., Deng, L., Dong, A., 2017. Preparation, pharmacokinetics, tissue distribution and antitumor effect of sorafenib-incorporating nanoparticles in vivo. Oncol. Lett. 14, 6163–6169. https://doi.org/10.3892/ol.2017.6934

Song, W., Ren, L., Lu, L., Xin, Y., Wang, K., Zhao, W., Su, Y., Tian, J., Li, Y., 2018. Sorafenib-loaded polymeric micelles as passive targeting therapeutic agents for hepatocellular carcinoma therapy. Nanomedicine 13, 1009–1023. https://doi.org/10.2217/nnm-2018-0046

Steichen, S.D., Caldorera-Moore, M., Peppas, N.A., 2013. A review of current nanoparticle and targeting moieties for the delivery of cancer therapeutics. Eur. J. Pharm. Sci. 48, 416–427. https://doi.org/https://doi.org/10.1016/j.ejps.2012.12.006

Tang, X., Chen, L., Li, A., Cai, S., Zhang, Y., Liu, X., Jiang, Z., Liu, X., Liang, Y., Ma, D., 2018. Anti-GPC3 antibody-modified sorafenib-loaded nanoparticles significantly inhibited HepG2 hepatocellular carcinoma. Drug Deliv. 25, 1484–1494. https://doi.org/10.1080/10717544.2018.1477859

van Rijt, S.H., Bein, T., Meiners, S., 2014. Medical nanoparticles for next generation drug delivery to the lungs. Eur. Respir. J. 44, 765 LP-774.

https://doi.org/10.1183/09031936.00212813

Wicki, A., Witzigmann, D., Balasubramanian, V., Huwyler, J., 2015. Nanomedicine in cancer therapy: Challenges, opportunities, and clinical applications. J. Control. Release 200, 138–157. https://doi.org/https://doi.org/10.1016/j.jconrel.2014.12.030

Wilhelm, S., Carter, C., Lynch, M., Lowinger, T., Dumas, J., Smith, R.A., Schwartz, B., Simantov, R., Kelley, S., 2006. Discovery and development of sorafenib: a multikinase inhibitor for treating cancer. Nat. Rev. Drug Discov. 5, 835.

Yamazaki, M., Ito, T., 1990. Deformation and instability of membrane structure of phospholipid vesicles caused by osmophobic association: mechanical stress model for the mechanism of poly(ethylene glycol)-induced membrane fusion. Biochemistry 29, 1309–1314. https://doi.org/10.1021/bi00457a029

Yuan, H., Chen, C.-Y., Chai, G., Du, Y.-Z., Hu, F.-Q., 2013. Improved Transport and Absorption through Gastrointestinal Tract by PEGylated Solid Lipid Nanoparticles. Mol. Pharm. 10, 1865–1873. https://doi.org/10.1021/mp300649z

Zhang, Y., Huo, M., Zhou, J., Xie, S., 2010. PKSolver: An add-in program for pharmacokinetic and pharmacodynamic data analysis in Microsoft Excel. Comput. Methods Programs Biomed. 99, 306–314. https://doi.org/https://doi.org/10.1016/j.cmpb.2010.01.007

Zhang, Z., Niu, B., Chen, J., He, X., Bao, X., Zhu, J., Yu, H., Li, Y., 2014. The use of lipid-coated nanodiamond to improve bioavailability and efficacy of sorafenib in resisting metastasis of gastric cancer. Biomaterials 35, 4565–4572. https://doi.org/10.1016/j.biomaterials.2014.02.024

Table 1: Physicochemical characterization of empty solid lipid nanoparticles (BSLN), sorafenib loaded nanoparticles (SSLN) and galactose-conjugated SSLN (mean ± standard deviation; n = 3).

Formulation	Particle size (d.nm)	Polydispersity index	Zeta potential (mV)	Drug encapsulation efficiency (%)
BSLN	**59.31±2.99**	**0.209±0.022**	**-20.9±1.41**	**-**
SSLN	**68.36±3.14**	**0.228±0.012**	**-20.13±1.35**	**97±1.5**
GAL-SSLN	**111±6.99**	**0.354±0.024**	**-19.8±1.11**	**95±1.8**

Table 2: Half maxillary inhibitory concentration (IC50) values of sorafenib (SRFB), SRFB loaded nanoparticles (SSLN) and galactose conjugated SSLN (GAL-SSLN) against HepG2 human hepatocellular carcinoma cell line after 48 h of incubation.

Formulation	IC50 at 48h (µg/ml)
SRFB	**9.48±0.45**
BSLN	**> 100 (193.70±1.46)**
SSLN	**9.77±1.47[a]**
GAL-SSLN	**6.57±0.58[*]**

* represents comparison between SRFB *vs* SSLN and GAL-SSLN. [a] represents insignificant difference in comparison with SRFB.

Table 3: Pharmacokinetic parameters of sorafenib (SRFB), sorafenib loaded SLN (SSLN), galactose conjugated sorafenib loaded SLN (GAL-SSLN).

PK Parameter	Unit	SRFB	SSLN	GAL-SSLN
C max	µg/ml	6.75±1.07	25.22±0.50***	28.90±0.13$^{***, \#\#}$
t max	h	1.17±0.28	4.00±0.00***	6.00±0.00$^{***, \#\#\#}$
AUC $_{0-t}$	µg/ml*h	32.59±2.98	272.05±30.60***	363.09±32.74$^{***, \#}$
AUC $_{0-\alpha}$	µg/ml*h	45.88±3.87	357.20±25.35***	598.92±36.28$^{***, \#\#\#}$
AUMC $_{0-\alpha}$	µg/ml*h^2	326.10±23.78	6723.35±52.36**	14896.37±496.08$^{***, \#\#}$
MRT	h	6.58±0.58	16.65±3.64**	26.49±1.58$^{***, \#}$
Clearance	(µg/ml)/h	0.55±0.04	0.07±0.004***	0.03±0.01$^{***, a}$
$t_{1/2}$	h	4.36±0.20	14.07±0.06***	16.75±1.09$^{***, \#}$

C_{max} = peak plasma concentration, t_{max} = time to reach peak plasma concentration, AUC = area under the curve, AUMC = area under the first moment curve, MRT = mean residence time, $t_{1/2}$ = plasma half life. Data represented as mean ± SD, n = 3 (* represents comparison of SRFB with SSLN, # represents comparison of SRFB with GAL-SSLN, ^{a} indicates insignificant difference and */ # $p < 0.05$, **/ ## $p < 0.01$ and ***/### $p < 0.001$).

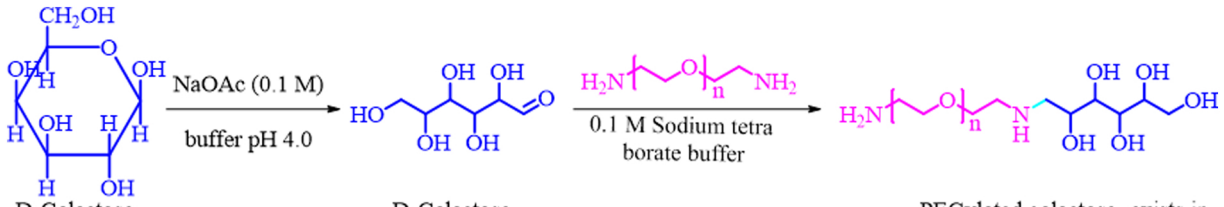

D-Galactose ring form

D-Galactose open chain

PEGylated galactose- exists in equilibrium with Schiff base

Figure 1

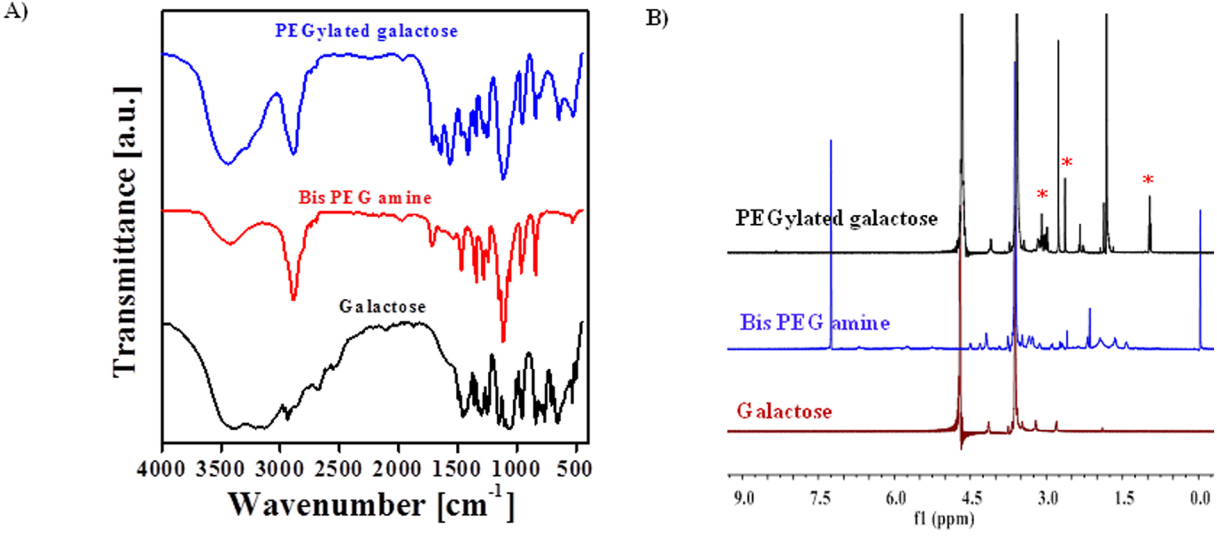
A)
PEGylated galactose
Bis PEG amine
Galactose
Transmittance [a.u.]
4000 3500 3000 2500 2000 1500 1000 500
Wavenumber [cm-1]
B)
PEGylated galactose
Bis PEG amine
Galactose
*
*
*
9.0 7.5 6.0 4.5 3.0 1.5 0.0
f1 (ppm)

Figure 2

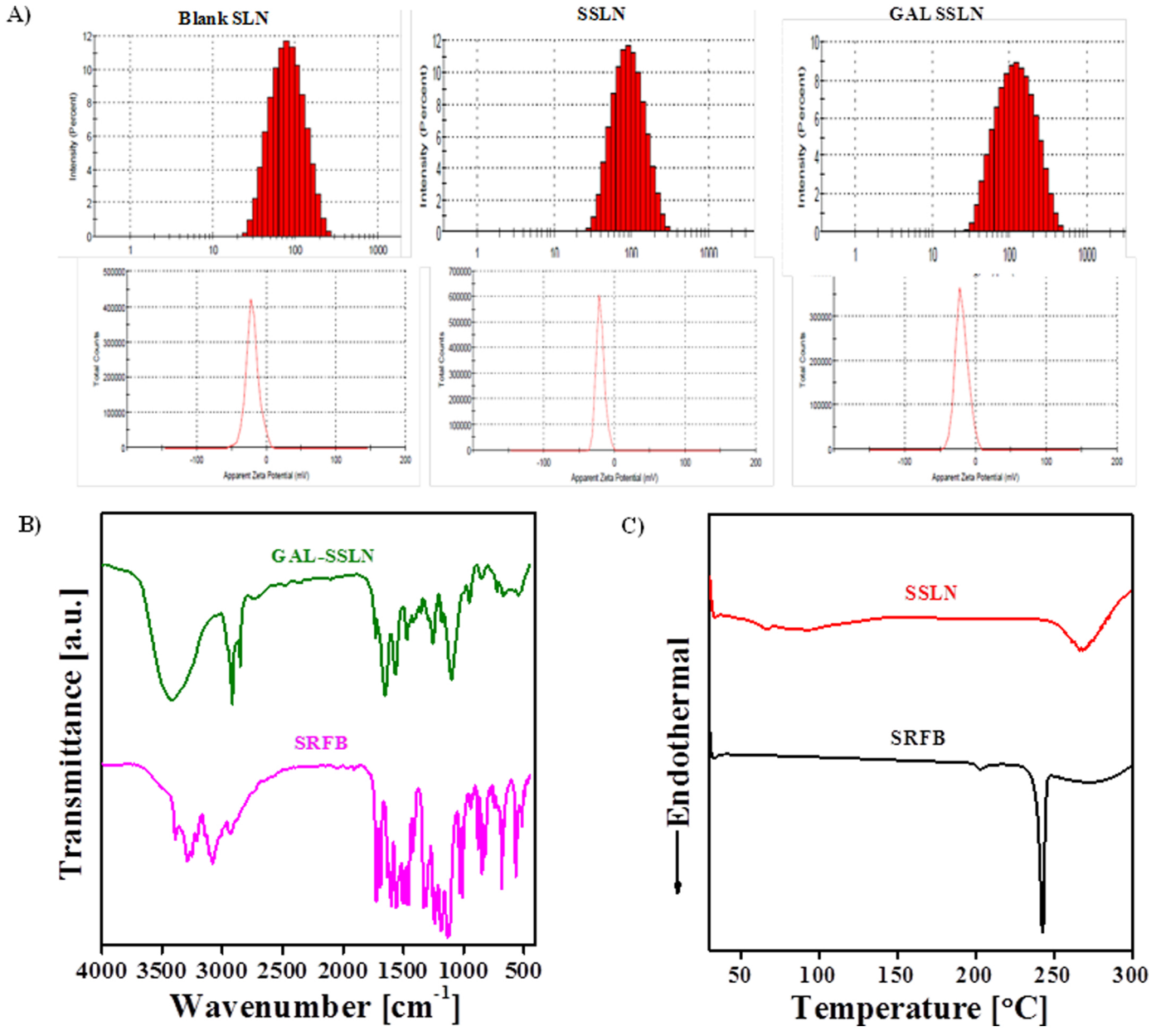
A)
Blank SLN
SSLN
GAL SSLN
Intensity (Percent)
Total Counts
Apparent Zeta Potential (mV)
B)
GAL-SSLN
SRFB
Transmittance [a.u.]
4000 3500 3000 2500 2000 1500 1000 500
Wavenumber [cm-1]
C)
SSLN
SRFB
Endothermal
50 100 150 200 250 300
Temperature [°C]

Figure 3

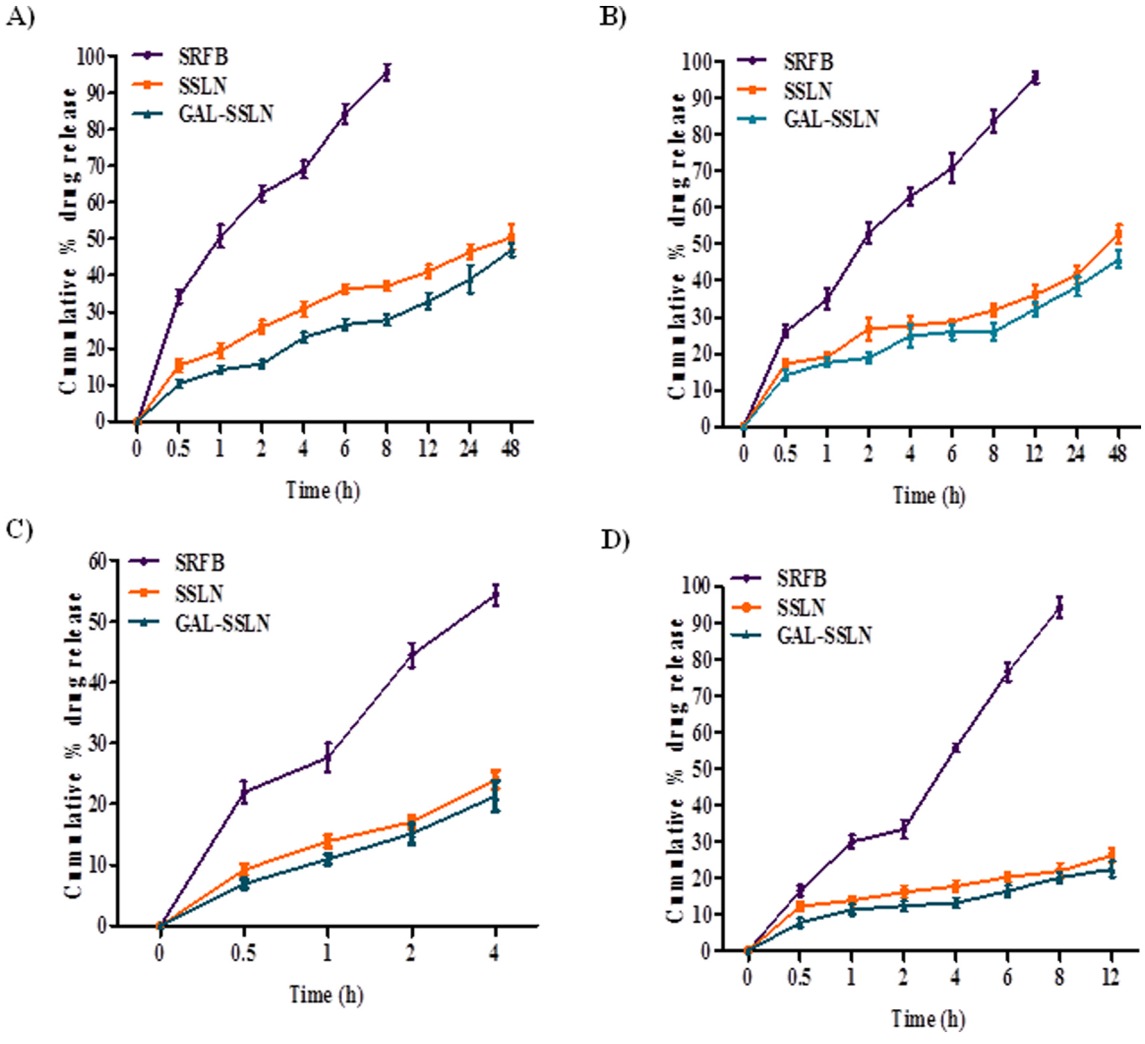
A)
SRFB
SSLN
GAL-SSLN
Cumulative % drug release
Time (h)
0 0.5 1 2 4 6 8 12 24 48
B)
SRFB
SSLN
GAL-SSLN
Cumulative % drug release
Time (h)
0 0.5 1 2 4 6 8 12 24 48
C)
SRFB
SSLN
GAL-SSLN
Cumulative % drug release
Time (h)
0 0.5 1 2 4
D)
SRFB
SSLN
GAL-SSLN
Cumulative % drug release
Time (h)
0 0.5 1 2 4 6 8 12

Figure 4

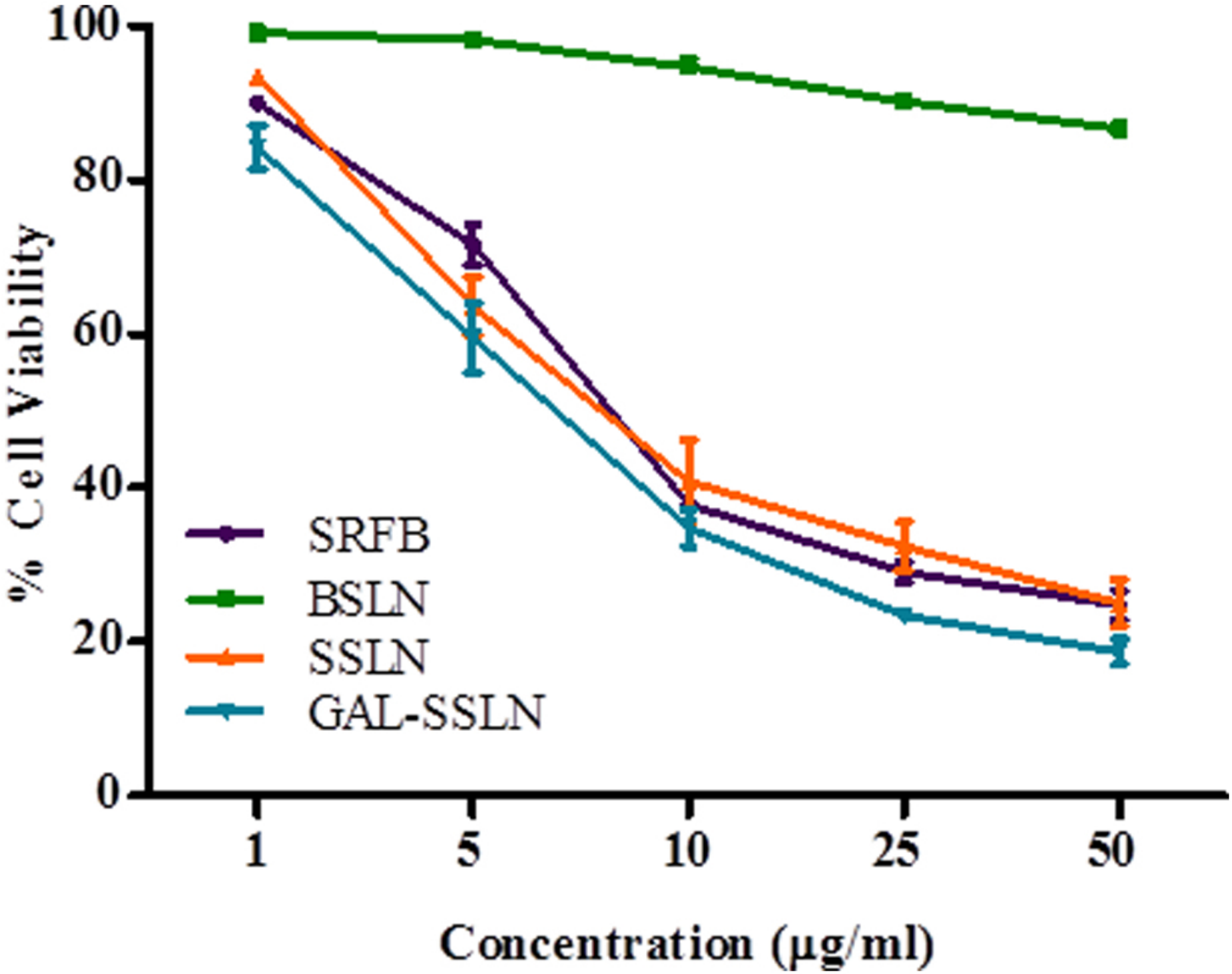
100
80
60
40
20
0
% Cell Viability
SRFB
BSLN
SSLN
GAL-SSLN
1
5
10
25
50
Concentration (µg/ml)

Figure 5

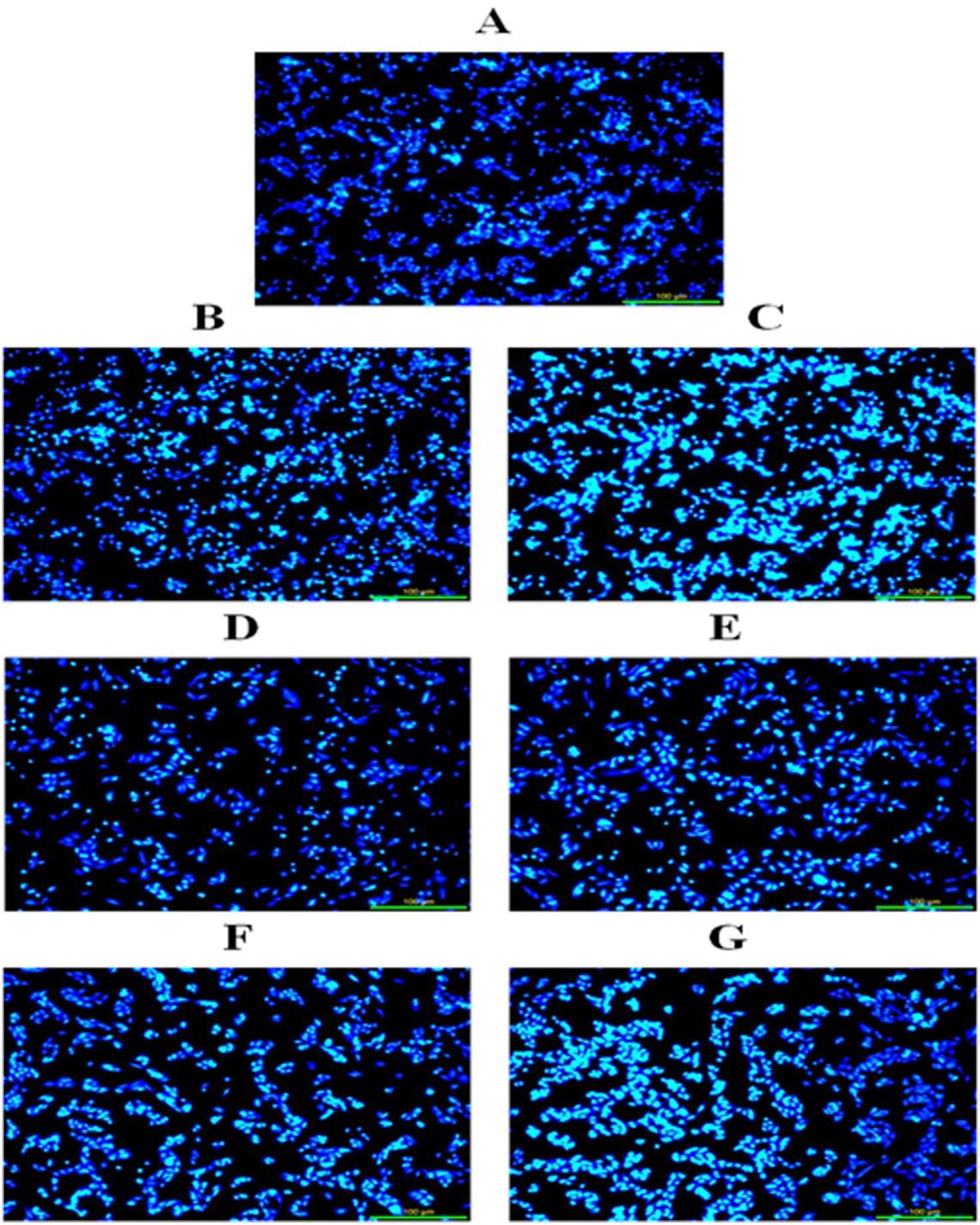

Figure 6

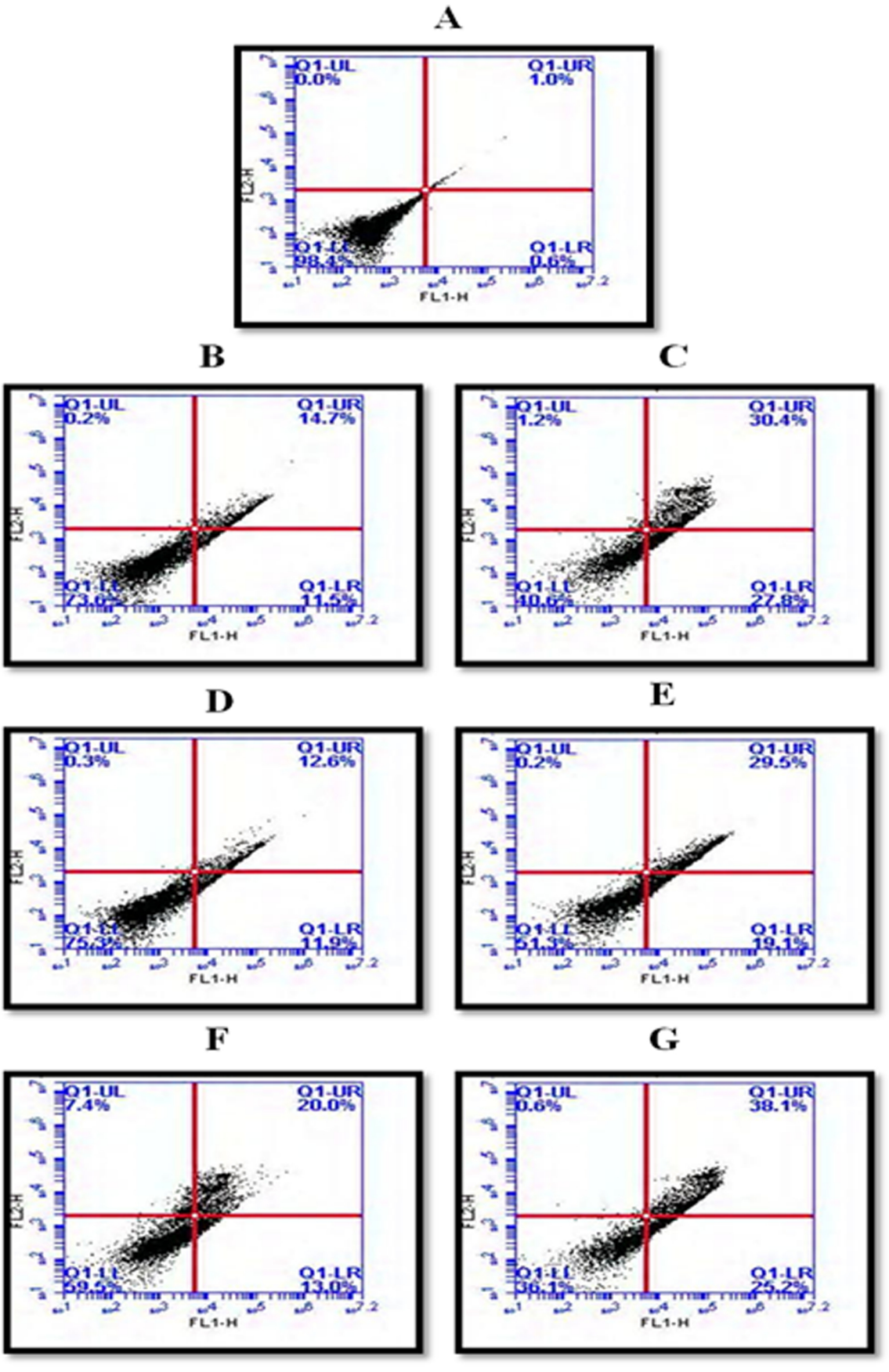
A
Q1-UL
0.0%
Q1-UR
1.0%
Q1-LL
98.4%
Q1-LR
0.6%
FL2-H
FL1-H
B
Q1-UL
0.2%
Q1-UR
14.7%
Q1-LL
73.6%
Q1-LR
11.5%
FL2-H
FL1-H
C
Q1-UL
1.2%
Q1-UR
30.4%
Q1-LL
40.6%
Q1-LR
27.8%
FL2-H
FL1-H
D
Q1-UL
0.3%
Q1-UR
12.6%
Q1-LL
75.3%
Q1-LR
11.9%
FL2-H
FL1-H
E
Q1-UL
0.2%
Q1-UR
29.5%
Q1-LL
51.3%
Q1-LR
19.1%
FL2-H
FL1-H
F
Q1-UL
7.4%
Q1-UR
20.0%
Q1-LL
69.5%
Q1-LR
13.0%
FL2-H
FL1-H
G
Q1-UL
0.6%
Q1-UR
38.1%
Q1-LL
36.1%
Q1-LR
25.2%
FL2-H
FL1-H

Figure 7

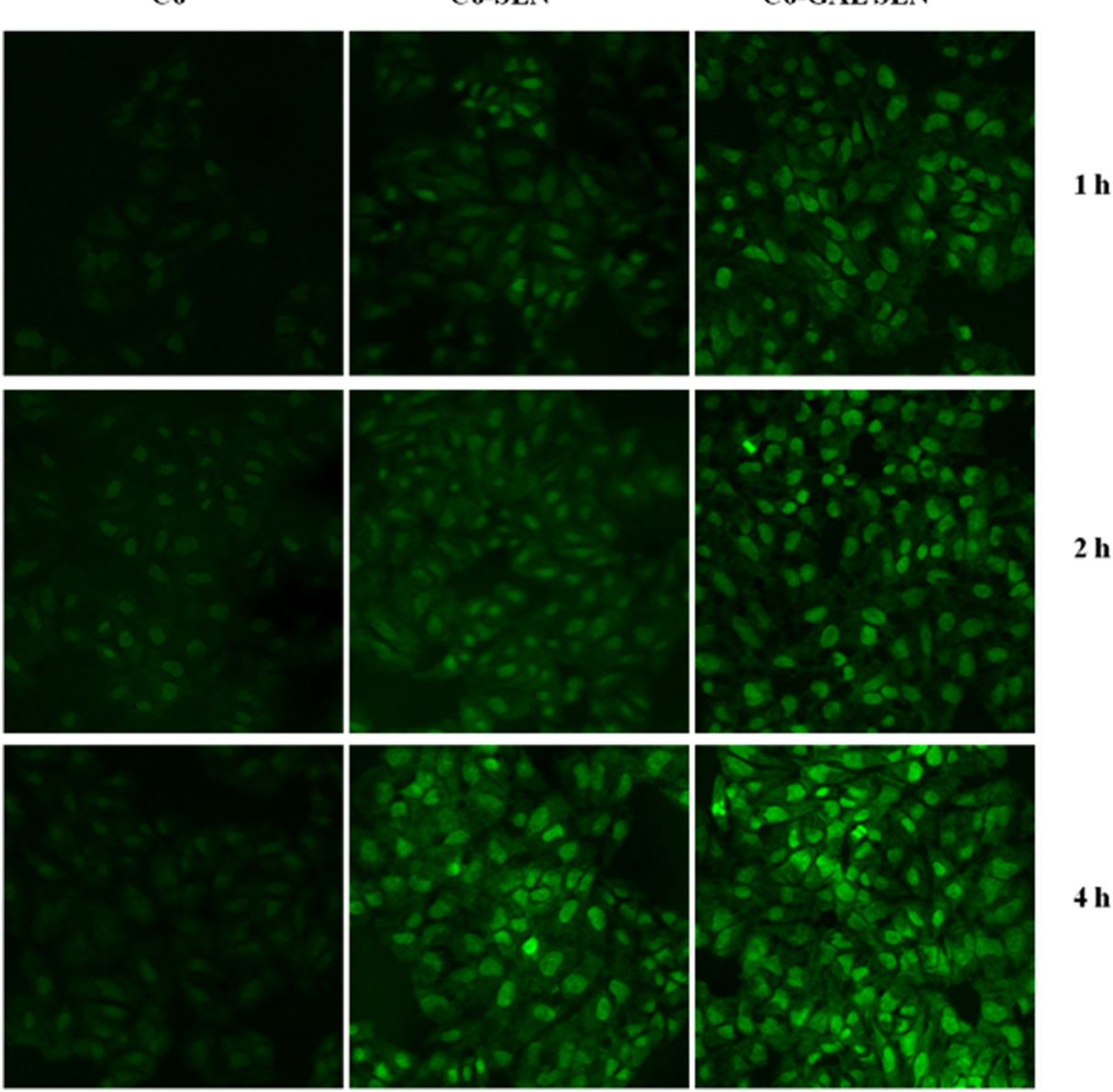

Figure 8

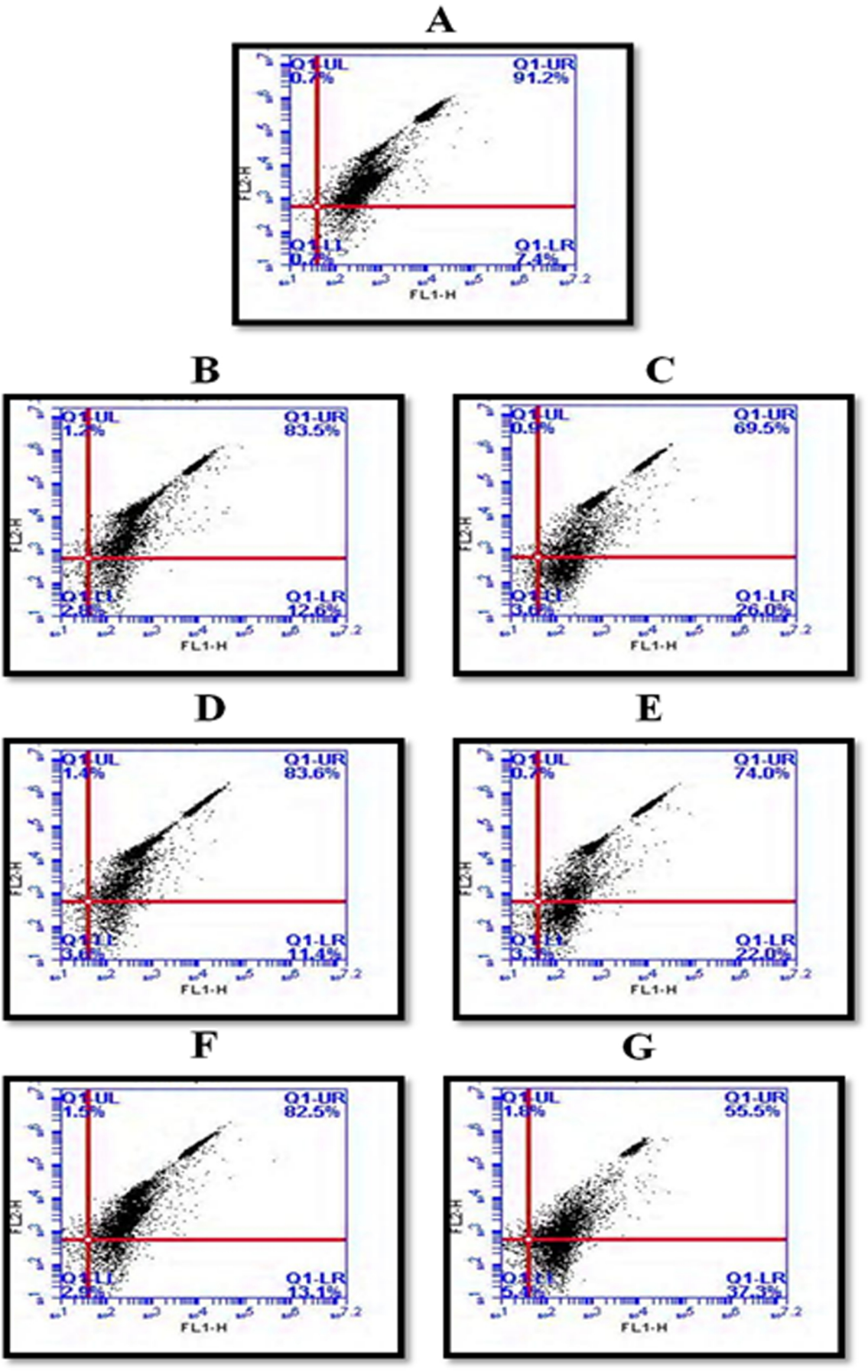
A
Q1-UL
0.7%
Q1-UR
91.2%
Q1-LL
0.7%
Q1-LR
7.4%
FL2-H
FL1-H
B
Q1-UL
1.2%
Q1-UR
83.5%
Q1-LL
2.8%
Q1-LR
12.6%
FL2-H
FL1-H
C
Q1-UL
0.9%
Q1-UR
69.5%
Q1-LL
3.6%
Q1-LR
26.0%
FL2-H
FL1-H
D
Q1-UL
1.4%
Q1-UR
83.6%
Q1-LL
3.6%
Q1-LR
11.4%
FL2-H
FL1-H
E
Q1-UL
0.7%
Q1-UR
74.0%
Q1-LL
3.3%
Q1-LR
22.0%
FL2-H
FL1-H
F
Q1-UL
1.5%
Q1-UR
82.5%
Q1-LL
2.9%
Q1-LR
13.1%
FL2-H
FL1-H
G
Q1-UL
1.8%
Q1-UR
55.5%
Q1-LL
5.4%
Q1-LR
37.3%
FL2-H
FL1-H

Figure 9

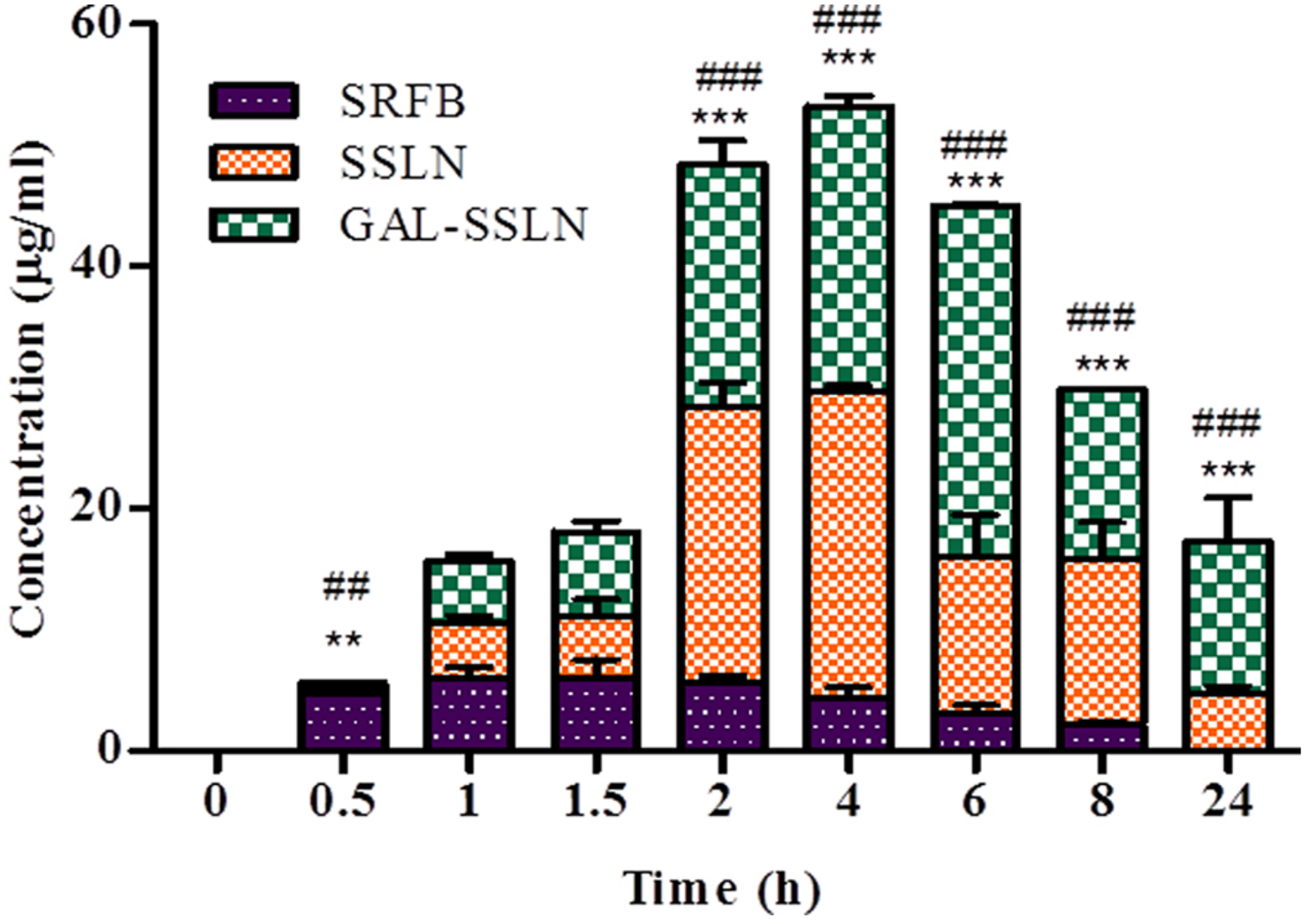
60
40
20
0
Concentration (µg/ml)
SRFB
SSLN
GAL-SSLN
##
**
###
***
###
***
###
***
###
***
###
***
0
0.5
1
1.5
2
4
6
8
24
Time (h)

Figure 10

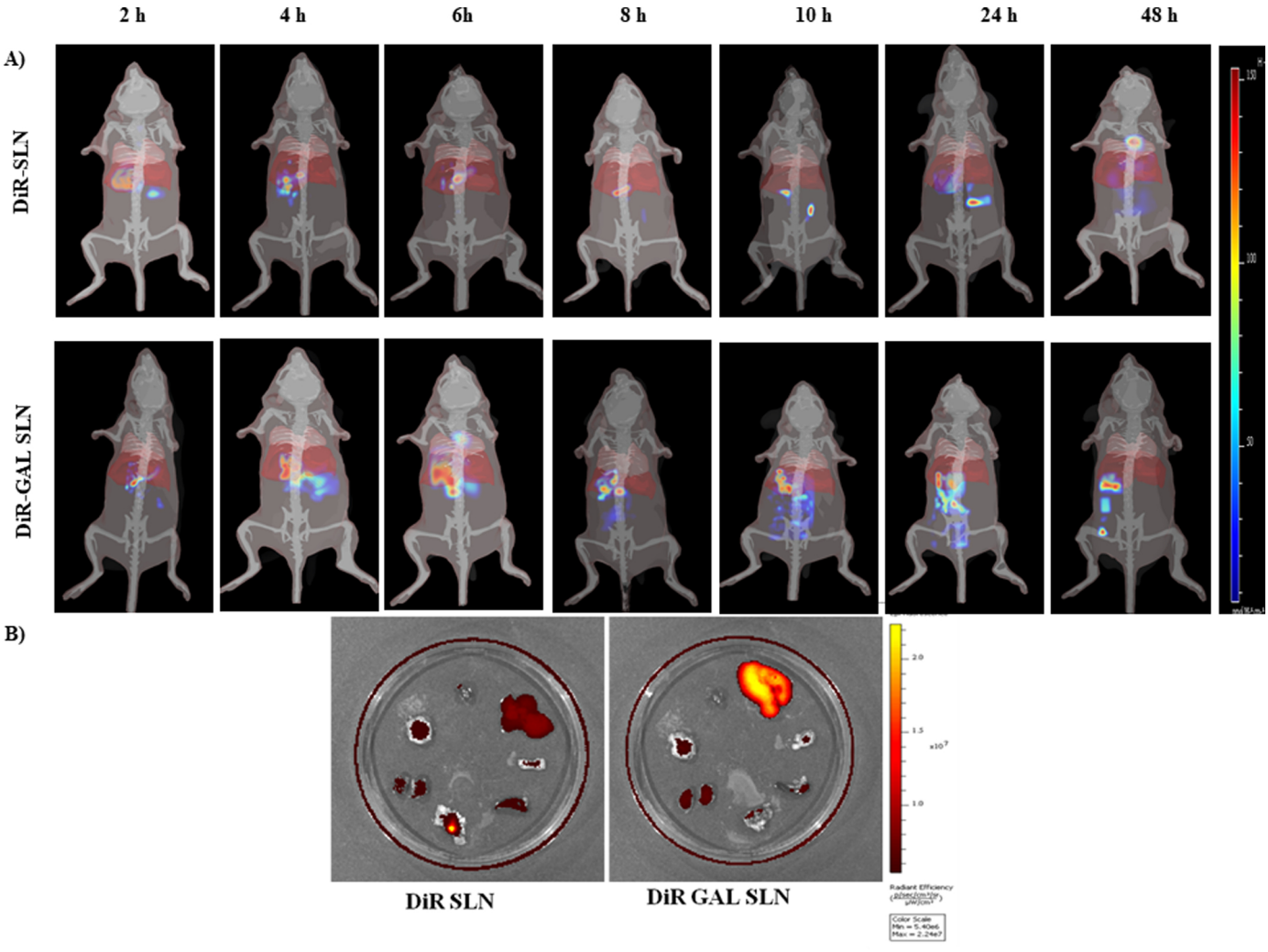
2 h
4 h
6h
8 h
10 h
24 h
48 h
A)
DiR-SLN
DiR-GAL SLN
B)
DiR SLN
DiR GAL SLN
Radiant Efficiency
Color Scale

Figure 11